Sedimentary insights into organic matter alteration in Arctic Alaska's saline permafrost

Fabian Seemann[1,2,3], Michael Zech[3], Maren Jenrich[1], Guido Grosse[1,2], Benjamin M. Jones[4], Claire Treat[5], Lutz Schirrmeister[1], Susanne Liebner[6,7] and Jens Strauss[1]

[1]Permafrost Research Section, Alfred Wegener Institute Helmholtz Centre for Polar and Marine Research, 14473 Potsdam, Germany
[2]Institute of Geosciences, University of Potsdam, 14467 Potsdam, Germany
[3]Institute of Geography, Technische Universität Dresden, 01069 Dresden, Germany
[4]Institute of Northern Engineering, University of Alaska Fairbanks, Fairbanks, Alaska 99775, USA
[5]Department of Agroecology, Aarhus University, 8000 Aarhus, Denmark
[6]Institute of Biochemistry and Biology, University of Potsdam, 14467 Potsdam, Germany
[7]GFZ Helmholtz Centre for Geosciences, Section Geomicrobiology, 14473 Potsdam, Germany

Correspondence to: Fabian Seemann (fabian.seemann@awi.de)

Abstract. In Arctic coastal lowland regions such as northernmost Alaska, thermokarst landscapes are often underlain by saline deposits, a factor frequently overlooked when assessing permafrost thaw risks. To evaluate the influence of thaw and salinity on organic matter degradation and landscape dynamics, we analyzed six sediment cores from representative landforms near Utqiaġvik (Alaska) using a multiproxy, carbon-focused approach, with emphasis on *n*-alkane biomarkers. Undisturbed tundra uplands contained well-preserved, organic-rich Holocene sediments (~140 cm thick) overlying brackish late Pleistocene deposits, indicating the presence of saline permafrost. Thermokarst lake subsidence into these substrates led to enhanced organic matter degradation, as reflected by lower *n*-alkane carbon preference index (CPI) values. While West Twin Lake talik sediments exhibited brackish porewater, East Twin Lake sediments were characterized by predominantly saline porewater, indicating the presence of a cryopeg driven by salt-induced thaw-point depression. Lagoonal environments, receiving both terrestrial and lacustrine inputs, accumulate sediments under unfrozen hypersaline conditions, presenting a high potential for organic matter decomposition. Carbon proxy signatures statistically distinguish perennially frozen uplands, unfrozen lake sediments, refrozen drained lake basins, and lagoonal settings. Our results demonstrate that salt-bearing deposits, as found in all investigated sites, are vulnerable to active layer deepening, talik and cryopeg formation, and lake/coastal shoreline erosion. These processes accelerate organic matter degradation and alter landscape trajectories. Our study underscores the need to better understand the role of saline permafrost in Arctic coastal lowlands and its broader implications under ongoing climate change.

1 Introduction

Arctic amplification is warming the polar north almost four times as fast as the global mean (Chylek et al., 2022; Rantanen et al., 2022). This amplification contributes to permafrost warming, increasing active layer depths, and a shrinking permafrost

extent, which relates almost linearly to global warming (Biskaborn et al., 2019; Liu et al., 2024; McGuire et al., 2016; Nitzbon et al., 2024; Smith et al., 2022). With ~1460–1600 gigatons the terrestrial permafrost region stores about three times as much organic carbon as global vegetation, which is vulnerable to mineralization with warming temperatures and permafrost thaw (Schuur et al., 2022; Strauss et al., 2025).

On vast Arctic coastal plains, like in northern Alaska, permafrost thaw manifests in several types of landforms, including thermokarst lakes and lagoons. Thermokarst processes are accelerating in the Alaskan tundra (Chen et al., 2021), and Nitze et al. (2017) describe a concurrent trend of thermokarst lake drainage. In drained lake basins (DLBs), permafrost starts to re-aggrade, but as the climate continues to warm, taliks (unfrozen areas) may increasingly remain in the sediments (Farquharson et al., 2022; Jones et al., 2022; Lantz et al., 2022).

Saline permafrost sediments are present under Holocene deposits on Arctic coastal plains, like in Alaska, Canada and Siberia (Brigham-Grette and Hopkins, 1995; Brouchkov, 2002, 2003; Eisner et al., 2005; Osterkamp, 1989). In these sediments, which were deposited during past marine transgressions, the freezing point of pore ice is depressed due to the high salt content, leading to a higher vulnerability to ground warming. When unfrozen cryotic deposits are present (i.e., unfrozen sediments at temperatures below the freezing point), these are referred to as cryopegs (van Everdingen, 2005). Jones et al. (2023) for example observed intensified permafrost degradation as a thermokarst lake subsided into saline deposits. Such trajectories are critical as the mobilization of previously freeze-locked organic matter occurs earlier than under non-saline conditions, potentially enhancing carbon mineralization and greenhouse gas production in saline permafrost regions.

Along the coastlines, the combination of sea-level rise and erosion leads to significant land loss, altering the carbon cycle and with that also greenhouse gas dynamics (Creel et al., 2024; Irrgang et al., 2022; Jenrich et al., 2024, 2025a; Nielsen et al., 2022; Vonk et al., 2025). Coastal and gully erosion can lead to thermokarst lake drainage into the ocean but may also open up lakes and turn them into new thermokarst lagoons (Arp et al., 2010; Jenrich et al., 2021; Jones et al., 2020). The importance of such transitional environments is demonstrated by the abundance of lagoons along some coasts. For example, more than 70 % of the Alaskan Beaufort Sea coastline is characterized by both thermokarst and non-thermokarst lagoons (Harris et al., 2017; Jenrich et al., 2025b).

To understand potential carbon losses due to permafrost degradation in such transitional landscapes, we need to understand sediment properties from these complex and dynamic systems that are characterized by regular or saline permafrost and diverse permafrost histories. On this issue, Giest et al. (2025) recently quantified a stronger organic matter degradation signal (in the context of microbial transformation toward a more mature state) in saline deposits compared to non-salt-influenced sites by utilizing using lipid biomarkers. Since coastal permafrost regions can vary substantially in their salinity - between fresh and hypersaline porewater conditions - (Jenrich et al., 2021), more differentiated investigations across different salinity levels are needed. Organic carbon proxies such as organic carbon to nitrogen ratios (C:N), organic carbon isotopes ($\delta^{13}C$, ^{14}C) and hydrocarbons (*n*-alkanes) are known to reflect organic matter origin and its degradation state, making them useful tools in tracing paleoenvironmental change and present carbon dynamics in permafrost regions (e.g., Giest et al., 2025; Goñi et al., 2000; Strauss et al., 2015). Organic matter quality - in the sense of its future degradation potential - can, for example,

be assessed by the *n*-alkane carbon preference index (CPI), a proxy that is increasingly applied in permafrost carbon studies (e.g., Andersson et al., 2012; Haugk et al., 2022; Martens et al., 2023; Yang et al., 2023).

In this study, we investigate the transformation of organic matter during permafrost degradation by studying core samples from a drilling transect along thaw and salinity gradients encompassing a diverse talik- and cryopeg-affected thermokarst terrain in Arctic Alaska. Accordingly, we address the following research questions: (1) which paleoenvironmental and modern processes and conditions shape today's sediment characteristics, (2) what is the organic matter quality in thermokarst landforms on the Utqiaġvik Peninsula, and (3) how do landscape dynamics affect organic matter mobilization? To achieve this, we employ a sedimentary organic carbon-centered multiproxy approach, including the aforementioned parameters.

2. Material and methods

2.1 Study area

The study area lies ca. 10 km east of Utqiaġvik (formerly Barrow; 71.276369, -156.452961; Fig. 1). The Utqiaġvik Peninsula covers an area of about 1800 km² (Lara et al., 2020). Geomorphologically, it is part of the Younger Outer Coastal Plain, which belongs to the Arctic Coastal Plain (Hinkel et al., 2005).

In the period 2016-2020, the mean annual air temperature was -7.8 °C and the mean annual precipitation was 200 mm. Both variables have been experiencing an increasing trend between 1981 and 2020 by 1.1 °C decade^{-1} and 23.1 mm decade^{-1}, respectively (Rawlins, 2021). The landscape is characterized by continuous permafrost with mean annual ground temperatures of approx. -6 °C at the permafrost table (Obu et al., 2019). The permafrost thickness is about 400 m (Brown et al., 2003) and the active layer (late season thaw) depth in Utqiaġvik ranged between 29 cm and 47 cm in the monitoring period 1995-2019 (Nyland et al., 2021).

The ecoregion of the study area is Arctic Tundra (Lara et al., 2025). Tundra uplands (primary or remnant surfaces) are shaped by high-centered polygons. High and flat centered polygons are dominated by graminoids, sedges and dwarf shrubs. Wet and seasonally flooded positions such as DLBs and troughs are predominantly characterized by graminoid species, sedges and *Sphagnum* mosses (Eisner et al., 2005; Lara et al., 2015; Wolter et al., 2024). The soil consists of ice- and organic-rich Holocene deposits, which are underlain by late Pleistocene sandy and silty marine sediments (Eisner et al., 2005). These saline sediments accumulated when sea levels were higher compared to today (Brigham-Grette and Hopkins, 1995; Brouchkov, 2003). The Cretaceous bedrock consists of sedimentary rock (Black, 1964).

Thermokarst lakes cover about 22 % and DLBs 50 % of the landscape (Hinkel et al., 2003; Jones et al., 2022). Both lakes investigated in this study, West Twin Lake (1.3 km² surface area, 181 cm deep) and East Twin Lake (1.3 km² surface area, 175 cm deep) are characterized by floating ice regimes, yet West Twin Lake is a freshwater lake while East Twin Lake exhibits brackish water (Jones et al., 2023). In DLBs, permafrost reforms after lake drainage, initializing polygonal patterns while remnant ponds may remain (Andresen and Lougheed, 2015; Eisner et al., 2005; Jones et al., 2022; Ling and Zhang, 2004). The former lake of the DLB, which is investigated in this study, was estimated to have drained about 100-150 years

ago following coastal erosion (Brown et al., 2003). The erosion rate of Elson Lagoon north and east of the investigated terrestrial sites is 0.3-5.0 m yr^{-1} (Gibbs and Richmond, 2017; Osterkamp and Harrison, 1985). South of the DLB a semi-open thermokarst lagoon (0.8 km^2, 94 cm deep) is fed by multiple streams (Fig. 1). Elson Lagoon itself is a large (125 km^2) but shallow (< 4 m) coastal lagoon with active deposition processes occurring (Zimmermann et al., 2022). Subsea permafrost exists beneath hypersaline lagoon sediments (Osterkamp and Harrison, 1982, 1985). The Barrow spit as well as barrier islands mark the transition to the Alaskan Beaufort Sea (Brown et al., 2003; Zimmermann et al., 2022).

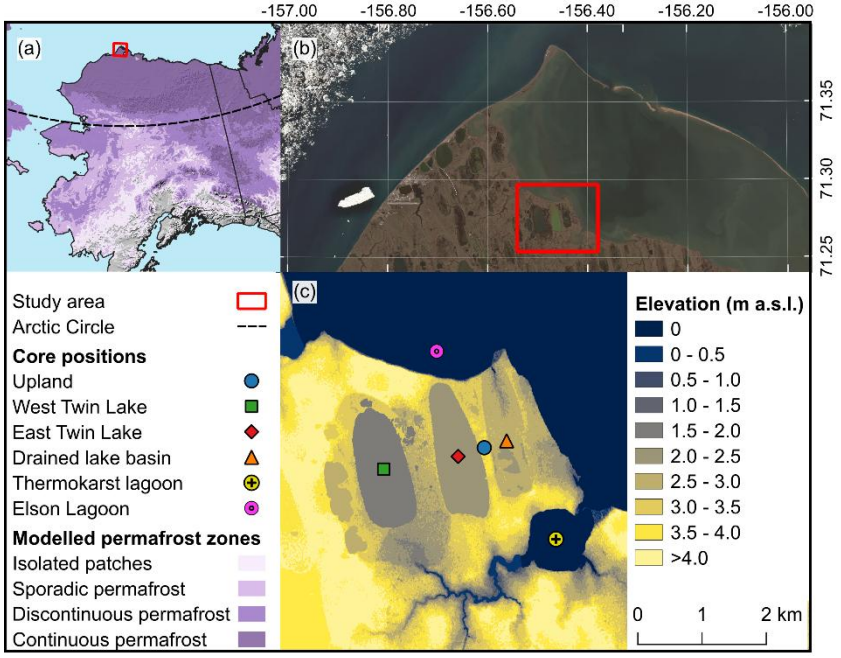

Figure 1: The study area located close to Utqiaġvik at the North Slope of Alaska. (a) Alaskan permafrost extent map based on data from Obu et al. (2018), (b) Copernicus (2023) Sentinel-2 LA satellite image of the Utqiaġvik Peninsula and Elson Lagoon, and (c) IFSAR digital terrain model (DGGS, 2018) with location of the coring sites.

2.2 Methods

2.2.1 Fieldwork

Sediment coring took place in April 2022. As the objective was to determine the transformation of organic matter during permafrost thaw along a thaw and salt transect, coring positions were chosen from the least thaw and salt affected location, the upland, to the most thaw and salt affected sites, the lagoons. Fieldwork aimed at sampling near-surface and deep (> 1 m) sediments, which was reached with the exception of coring at West Twin Lake (23 cm) and the semi-open thermokarst lagoon (46 cm). Detailed characteristics of core sites and metadata are provided in Table S1. Depending on the sediment conditions, three different coring devices were used. Frozen material from the upland and the DLB sites were cored with a "Snow, Ice and Permafrost Establishment" (SIPRE) corer. Since bedfast ice was present at Elson Lagoon and the semi-open

thermokarst lagoon, sediments were cored with a SIPRE corer, too. For transportation the cores were wrapped in plastic foil and stored frozen in thermoboxes.

Unfrozen sediments of West Twin Lake were cored using a push corer (UWITEC gravity corer). Additionally, to get deeper, East Twin Lake was sampled with a vibration coring system (Livingstone-type drive rod piston corer). These cores were kept unfrozen in their PVC (push core) and aluminium (vibra core) tubes in thermoboxes for transportation to AWI (Potsdam, Germany).

2.2.2 Multiproxy approach

In order to assess sediment characteristics along thaw and salinity gradients, a multiproxy approach was applied as individual organic matter proxies can be influenced by source heterogeneity, post-depositional alteration, and mixing of modern and reworked deposits (Diefendorf et al., 2011; Jong et al., 2024; Wu et al., 2022). Combining complementary proxies therefore allows robust interpretations of carbon sources, preservation states, and transformation processes.

Sample preparation

In preparation for the investigation of individual biogeochemical parameters, SIPRE cores were processed in a climate chamber at -8°C. The lake cores were prepared at 4 °C. All cores were cut in halves, cleaned, photographed, and described (sediment structures, color, cryostructures, Table S2-7). Subsequently, sediment cores were subsampled in adjusted steps (approx. 5 cm intervals) following the sediment structure, and weighted. With the exception of East Twin Lake, no artificial disturbances of the cores were observed.

Depth correction for vibra core compaction

During vibracoring of the East Twin Lake, especially sediments in the upper part of the lake deposits experienced compaction due to high water content and extended vibration time, while the lower sediments were more consolidated and subjected to less compaction. To correct the recovered core depths for compaction, a normalized exponential depth correction model was applied, following Athy's law of exponential porosity–depth decay (Athy, 1930) and approaches used in ocean drilling studies (Lisiecki and Herbert, 2007). The true sediment depth z_t was calculated from the measured depth z_m (in the core liner) using the formula:

$$z_t = D_p \times \frac{1-e^{-z_m/\lambda}}{1-e^{-L_c/\lambda}} \quad (1)$$

where D_p is the total penetration depth of the coring barrels (259 cm in this case), L_c is the total recovered core length (here 138 cm), and λ (lambda) is the exponential e-folding depth scale. The e-folding depth (λ) is defined as the characteristic depth over which a quantity decreases to 1/e (approximately 37%) of its initial value, assuming an exponential compaction.

In this study, λ represents the depth scale at which sediment compaction effectively reduces porosity or thickness by a factor of e due to vibration-induced consolidation. Based on previous studies of lakes, thermokarst properties were adapted (especially water content, grain size, and porosity, e.g., Walter Anthony et al., 2014), and λ = 50 cm was assumed, reflecting the highly compressible, water-rich upper layers. This correction ensures that the calculated true depth equals D_p at the base of the core and follows an exponential compaction trend consistent with observed porosity–depth profiles in similar sediments.

Porewater extraction and electrical conductivity measurements

All samples were kept at 4 °C. Porewater was extracted with Rhizon samplers (0.12-0.18 µm membrane pore size). The extracted waters were measured with an Orion VERSASTAR PRO (Thermo Fisher) for electrical conductivity (mS cm^{-1}). Salinity stages were adapted from Cahyadi et al. (2018) as follows: Freshwater < 1.5 mS cm^{-1}, brackish 1.5-15.0 mS cm^{-1}, saline 15.0-50.0 mS cm^{-1}, and hypersaline > 50 mS cm^{-1}. For subsequent sample treatment, the sediment remains were freeze-dried, and the water/ice contents (in weight %, wt%) were calculated by taking into account the wet and dry sample weights.

Sedimentology and elemental analyses

For the investigation of the grain size distribution, subsamples were treated with hydrogen peroxide for the removal of organic matter for four weeks. The grain sizes were measured with a Malvern Mastersizer 3000 (0.01–1000 µm grain size range) and evaluated with GRADISTAT 8.0 (Blott and Pye, 2001).

Using further subsamples, samples were milled and homogenized for the elemental analyses using a planetary mill (Fritsch PULVERISETTE 5). Using a soliTOC and a rapid N exceed element analyzer (Elementar), total organic carbon (TOC) and total nitrogen (TN) contents were quantified through the combustion and the analysis of the resulting gases. The detection limits of TOC and TN are 0.001 wt% and 0.05 wt%, respectively, however, the detection limit was artificially set to 0.1 wt% for both elements. TOC and TN contents below the detection limit (0.1 wt%) were replaced by half of the detection limit (0.05 wt%). This is to prevent a bias and is according to Strauss et al. (2022) to make the point that low measurements are not the same as no measurements, avoiding zero inflation. For the TN samples below the detection limit, no C:N ratio calculation was done to avoid artificial artifacts. The C:N ratio is a common indirect indicator of organic matter degradation if assuming a same source signal, with lower values reflecting higher decomposition (e.g., Fuchs et al., 2019; Mu et al., 2025). It also helps to infer source material, distinguishing algal input (C:N < 10) from terrestrial plant matter (C:N > 20) (Meyers, 1994).

Stable organic carbon isotope analysis

Samples were decarbonized with hydrochloric acid before quantification of $\delta^{13}C$ at the Alfred Wegener Institute's (AWI) ISOLAB facility. $\delta^{13}C$ ratios were measured using internationally certified reference materials obtained from the IAEA, including USGS-24 (-15.99 ‰) and IAEA-CH-7 (-31.80 ‰). In addition, internal laboratory standards (peptone (-24.09 ‰) and nicotinamide (-32.73 ‰)) were analyzed for quality control. Isotope values are reported in ‰ relative to Vienna Pee Dee Belemnite (Coplen et al., 2006), and analytical precision was better than ±0.15 ‰ based on repeated standard measurements (Schwamborn et al., 2023). Measurements were run on a ThermoFisher Scientific Delta-V-Advantage gas mass spectrometer equipped with a FLASH elemental analyser EA 2000 and a CONFLO IV gas mixing system. Stable carbon isotope ratios are commonly applied as a proxy for organic matter origin and degradation in permafrost regions (e.g., Alewell et al., 2011; Strauss et al., 2015).

Radiocarbon dating

Radiocarbon dating was conducted on 21 selected samples by accelerator mass spectrometry at the MICADAS radiocarbon laboratory at AWI Bremerhaven (Mollenhauer et al., 2021). Preferably, plant remains were picked for dating, however, bulk sediment was analyzed for four samples due to the lack of macrofossils (Table S8). Macrofossil material was subject to a standard acid–base–acid pre-treatment (Mollenhauer et al., 2021). Subsequently, samples were rinsed to neutral pH, dried, and combusted using an elemental analyzer. Owing to limited sample mass, all but two macrofossil samples (AWI MICADAS sample ID 12532.1.1 and 12535.1.1, Table S8) were analyzed in gas mode rather than as graphite targets. Radiocarbon measurements were normalized and blank-corrected using size-matched OxAII and PhA standards. Data quality was monitored using wood reference material (IAEA-C5) in parallel (Mollenhauer et al., 2021). The bulk solid phase samples were acidified three times in silver boats with 6 M HCl to remove inorganic carbon. Radiocarbon dating was performed on 1 mgC graphite targets. Sample treatment and blank determination was performed following existing protocols by Mollenhauer et al. (2021). Raw radiocarbon ages were calibrated with Calib 8.20 using the IntCal 20 calibration curve (Reimer et al., 2020; Stuiver and Reimer, 1993).

***n*-Alkane biomarkers**

The total lipid extract from freeze-dried, milled and homogenized sediment was extracted with a Dionex ASE 350 Accelerated Solvent Extractor using dichloromethane/methanol (DCM/MeOH, 99:1 v/v, heating phase 5 min, static phase 20 min at 75°C and 10 MPa). Next, the internal standard 5α-androstane was added to the extract. Asphaltenes were precipitated to avoid complications during the next step, where the *n*-alkane including aliphatic fraction was separated via medium pressure liquid chromatography using *n*-hexane over silica columns (Radke et al., 1980). This fraction was then measured using a Thermo Scientific ISQ 7000 Single Quadrupole Mass Spectrometer in combination with a Thermo Scientific Trace

1310 Gas Chromatograph (capillary column from BPX5, 2 mm × 50 m, 0.25 mm). With a total run time of 118 min, the MS transfer line temperature was set to 250 °C and the ion source temperature to 230 °C (ionisation energy 70 eV at 50 µA). Targeted screening of mid- and long chain *n*-alkanes (C_{23}-C_{33}) was realized with the software Xcalibur (Thermo Fisher). The mass spectra (*m/z* 50-600 Da, 2.5 scans s^{-1}) and the internal standard were used for compound specific identification and quantification.

n-Alkane proxies

The total *n*-alkane content (TAC) is the first proxy that is indicative of (paleo) environmental conditions and degradation effects (e.g., Brittingham et al., 2017; Thomas et al., 2021). TAC is provided for the following chain lengths in µg g^{-1} Sediment (Sed) and µg g^{-1} TOC:

$$TAC = \Sigma C_{23} - C_{33} \quad (2)$$

The average chain length (ACL), developed by Poynter and Eglinton (1990), is a proxy that is indicative of the organic matter source. Algae and microorganisms are typically dominated by short-chain *n*-alkanes (< C_{22}), aquatic (submerged/floating, e.g., *Sphagnum* moss) vegetation can be recognized by a dominance of mid-chain *n*-alkanes (C_{23}/C_{25}) while terrestrial vegetation is dominated by long-chain *n*-alkanes (> C_{25}) (Baas et al., 2000; Ficken et al., 2000; Killops and Killops, 2005; Otto and Simpson, 2005). Terrestrial vegetation can further be distinguished between shrubs and trees (C_{27}/C_{29} predominance) and grasses and herbs (C_{31}/C_{33} predominance) (Maffei, 1996; Schäfer et al., 2016). This chemotaxonomic "fingerprint", as Eglinton et al. (1962) put it, can therefore be used as a tool for past environmental changes (e.g., Schwark et al., 2002; Zech et al., 2010). ACL limitations concern the blindness towards gymnosperms, overlapping chemotaxonomic patterns of different source material and potential post depositional alteration through degradation (Diefendorf et al., 2011; Jongejans et al., 2020; Struck et al., 2018; Zech et al., 2021). The ACL is calculated following Brittingham et al. (2017) and others:

$$ACL_{C23-C33} = \frac{\Sigma\, i \times C_i}{\Sigma\, C_i} \quad (3)$$

Odd chain alkanes predominate over even chain numbers (Eglinton et al., 1962). The ratio of odd against even chain lengths, called CPI, was first developed by Bray and Evans (1965) and further developed by Marzi et al. (1993). With advancing organic matter decay this ratio decreases (e.g., Andersson and Meyers, 2012; Schäfer et al., 2016). The CPI values of algae, bacteria, and highly degraded substances such as oil approach one while less degraded organic matter retains values > 5 (Haugk et al., 2022; Killops and Killops, 2005; Tipple and Pagani, 2010). The CPI calculation is based on the formula introduced by Marzi et al. (1993) for the chain length interval C_{23}-C_{33}:

$$CPI_{C23-C33} = \frac{\Sigma\, odd\ C_{23-31} + \Sigma\, odd\ C_{25-33}}{2 \times \Sigma\, even C_{\ 24-32}} \quad (4)$$

To differentiate terrestrial vegetation between trees and shrubs (approaching 0), and grasses and herbs (approaching 1), the endmember model of Schäfer et al. (2016) is applied:

$$n-alkane\ ratio\ =\ \frac{C_{31}+C_{33}}{C_{27}+C_{31}+C_{33}} \quad (5)$$

Ficken et al. (2000) developed a proxy (P_{aq}) which allows to more specifically quantify the share of aquatic macrophyte input into the sedimentary record. Submerged/floating macrophytes reveal relatively high values ($P_{aq} > 0.4$) compared to emergent and terrestrial plants ($0.1 < P_{aq} < 0.4$; $P_{aq} < 0.1$; respectively). To evaluate aquatic influences in the continuum from the permafrost upland, over the thermokarst lakes and the drained basin, towards the lagoons, P_{aq} was applied accordingly:

$$Paq\ =\ \frac{C_{23}+C_{25}}{C_{23}+C_{25}+C_{29}+C_{31}} \quad (6)$$

2.2.3 Statistical approaches

The combination of the biogeochemical and hydrochemical parameters was used to interpret units along the sediment cores (described top-down, labelled in Roman numerals) to enhance clarity and facilitate understanding. Mean values are reported alongside their standard deviations. Correlations between geochemical variables were assessed using Pearson correlation analysis.

In order to statistically quantify the characteristics of organic matter parameters (TOC, C:N, $\delta^{13}C$) in different sediment regimes, groups of thermal conditions (*seasonally frozen*, perennially *frozen*, *unfrozen*, *refrozen*, *lagoon*) and salinity stages (*freshwater*, *brackish*, *saline*, *hypersaline*) were created. Due to violations of normality in multiple groups, as determined by Shapiro-Wilk tests, the non-parametric Kruskal-Wallis test was used to assess differences in TOC, C:N, and $\delta^{13}C$ among groups. For subsequent pairwise comparisons of the categories with the parameters, Mann-Whitney U tests were applied, coupled with the Benjamini-Hochberg (BH) p-value adjustment method. *n*-Alkane proxies were not included in the statistical tests due to limited sample counts in individual groups.

To quantify if any group statistically differs from another based on the combination of TOC, C:N, and $\delta^{13}C$, a Permutational Multivariate Analysis of Variance (PERMANOVA) was performed. Also, unique groups based on both their thermal and salinity condition were created and tested with a PERMANOVA. Following a significant overall result, post-hoc pairwise PERMANOVA tests were conducted with p-value adjustment (BH) to identify which specific groups differed. All statistical analyses were carried out in RStudio and AI tools have been utilized for R coding.

3. Results

3.1 Biogeochemistry of the individual cores

The following subchapters are organized according to their geomorphological position. Chapter 3.2, by contrast, is structured based on thermal and salinity differences.

3.1.1 Permafrost upland

The upland core from the tundra site is characterized by silt-dominated ice-rich permafrost in the first two meters of the soil column (on average 66.4±13.1 wt% ground ice; Fig. 2a). The electrical conductivity of the porewater indicates freshwater conditions (< 1.5 mS cm^{-1}) and a trend towards saline conditions (max. 17.3 mS cm^{-1}) below 140 cm depth (Unit VI). At 75 and 102 cm depth, radiocarbon dating reveals similar ages with 6.98 and 6.97 cal ka BP, respectively, while a lower sample at 186 cm depth has an age of 13.3 cal ka BP. This suggests that Holocene deposits with a thickness of at least 126 cm (7.3 cal ka BP) cover the underlying late Pleistocene sediments. The TOC contents range between 35.3 wt% (Unit I) and 5.6 wt% (Unit VI). Between 70 and 100 cm depth, TOC contents are increased (Unit IV) compared to sediments above and below. TN contents relate to TOC contents and range between 0.4 and 1.7 wt% (on average 0.7±0.3 wt%). Overall, the C:N ratio is relatively homogenous along the core (on average 17.1±2.9). In the upper meter (Unit I-IV), the ratio is increased (19.7±1.5) compared to the lower meter (14.4±0.5). Carbon isotopic values range from an average of -26.8±0.6 ‰ in the upper 48 cm (Units I, II) to -27.7±0.4 ‰ between 53 and 198 cm depth. C:N and $\delta^{13}C$ ($r = 0.78$, $p < 0.001$) correlate significantly (Fig. S1).

Total *n*-alkane contents in the upland indicate a decreasing trend with depth (average 42.0±37.1 µg g^{-1} Sed; 268.7±160.7 µg g^{-1} TOC; Fig. 3). The maximum content is found at 10 cm depth with 113.3 µg g^{-1} Sed (524.7 µg g^{-1} TOC) and the minimum at 186 cm depth with 5.1 µg g^{-1} Sed (89.3 µg g^{-1} TOC). Long-chain *n*-alkanes dominate (average ACL 26.9±0.6) and the degradation proxy CPI (average 15.1±4.4) reveals a distinct pattern. First, the CPI increases with depth from 10.6 to 21.5 (75 cm depth). Then, it drops to 10.0 (126 cm depth) and increases again to 15.6 (186 cm depth). The *n*-alkane ratio, indicative for different terrestrial vegetation inputs, increases along the core from 0.1 (uppermost sample) to 0.4 (lowermost sample). P_{aq} indicates aquatic influences with values between 0.4 and 0.7.

3.1.2 West Twin Lake

The pushcore of the West Twin Lake talik is 23 cm long (4 subsamples) and therefore represents the surface sediments of the thermokarst lake (Fig. 2b). The sediment consists of fine silt (mean grain size 4.8±0.2 µm) with porewater of slightly brackish conditions (1.9 mS cm^{-1}). TOC contents are on average 16.1±0.4 wt%, and TN values range from below detection limit to 0.9 wt%. This results in C:N ratios of 17.5 (8 cm depth), 17.4 (16 cm depth), and 18.9 (21 cm depth). The $\delta^{13}C$ ratio is on average -28.6±0.1 ‰.

One biomarker sample was analyzed at the West Twin Lake core at 8 cm depth (Fig. 3). The total alkane content is 192.2 µg g^{-1} Sed (1214.3 µg g^{-1} TOC) and is therefore higher than in the upland. On the other hand, the ACL (25.5) and CPI (6.9) are lower compared to the upland. The *n*-alkane ratio, signalizing terrestrial input into the lake, is 0.2, while the P_{aq} value is 0.8.

3.1.3 East Twin Lake

The sediments in the vibracore from the East Twin Lake are sandy to silty (Fig. 2c). Until 187 cm depth (Unit I, II) mean grain sizes increase to 68.6 µm, and below that they average 16.4±6.1 µm. The electrical conductivity continuously increases from brackish (14.1 mS cm^{-1} at 8 cm depth) to saline (43.3 mS cm^{-1} at 235 cm depth). Subsequently, the conductivity decreases but remains in saline conditions. At 41 cm depth, radiocarbon dating revealed a Holocene age of 2.9 cal ka BP. At 215 and 252 cm depth, the sediment is of late Pleistocene age, 27.7 cal ka BP and 42.6 cal ka BP, respectively (Unit III). The surface sediments have a TOC content of 16.0 wt% (Unit I). Subsequently, TOC decreases and remains < 3.0 wt% below 123 cm depth (Unit II, III). Only six out of 26 samples showed TN values above the detection limit. The TN content in these samples is 0.1-0.9 wt%. The resulting average C:N ratio is 9.9±6.1. Carbon isotopic values increase from a minimum of -28.9 ‰ at 41 cm depth to -25.7 ‰ at 197 cm depth. Below that, $\delta^{13}C$ values remain relatively homogenous until the core bottom at 258 cm with an average of -25.8±0.1 ‰. C:N and $\delta^{13}C$ ($r = -0.91$, $p = 0.01$) reveal a very strong negative correlation (Fig. S1).

The surface sediment sample of East Twin Lake has a TAC of 305.4 µg g^{-1} Sed (2179.2 µg g^{-1} TOC), while at 75 and 121 cm depth, it decreased to 1.9 µg g^{-1} Sed (129.7 µg g^{-1} TOC) and 17.0 µg g^{-1} Sed (1020.0 µg g^{-1} TOC), respectively (Fig. 3). Long-chain *n*-alkanes predominate (average ACL 26.0±0.5). CPI (average 6.2±0.8), *n*-alkane ratio (average 0.3±0.1), and P_{aq} (0.7±0.1) are similar as in West Twin Lake.

3.1.4 Drained lake basin

The DLB core comprises frozen silty sand (Fig. 2d). The permafrost is less ice-rich compared to the upland (on average 48.8±20.6 wt% ground ice), and the electrical conductivity indicates predominantly brackish porewater conditions until 110 cm depth (on average 3.7±3.1 mS cm^{-1}). The basal surface peat (21 cm depth, Unit I), an indication of the drainage event date, has an age of 0.7 cal ka BP. Between 74 and 108 cm depth, an age-depth inversion occurs with 10.5 and 9.9 cal ka BP, respectively. The first late Pleistocene age is found at 140 cm depth with 34.1 cal ka BP. TOC values range between 1.5 (129 cm depth) and 42.4 wt% (undecomposed surface peat). Between 74 and 113 cm depth (Unit IV), a cryoturbated sediment structure is found, which is characterized by organic-rich sediments (33.5 wt% TOC at 113 cm depth). The TN contents are in the range of contents found in the upland, but are on average slightly lower (0.5±0.4 wt%). The C:N ratios (on average 18.6±5.1) reflect the TOC and TN patterns along the core however, peak values (0-15 cm and 113 cm depth) are less dominant. The $\delta^{13}C$ values increase with depth and range between -29.4 and -25.0 ‰ at 3 and 137 cm depth, respectively. No significant correlation is found between C:N and $\delta^{13}C$ ($r = -0.35$, $p = 0.08$; Fig. S1).

Compared to all investigated landforms, *n*-alkane specific parameters indicate the strongest heterogeneity in the DLB (Fig. 3). TAC ranges between 0.9 µg g^{-1} Sed (38.6 µg g^{-1} TOC) and 519.8 µg g^{-1} Sed (3419.6 µg g^{-1} TOC), which is the lowest and highest observed value in our study, respectively. The minimum ACL (25.6 at 31 cm depth) is similar to the surface samples

of the lakes. At 108 cm depth, extreme values are reached for ACL (30.2), CPI (51.3), the terrestrial *n*-alkane ratio (0.9), and P_{aq} (0.02).

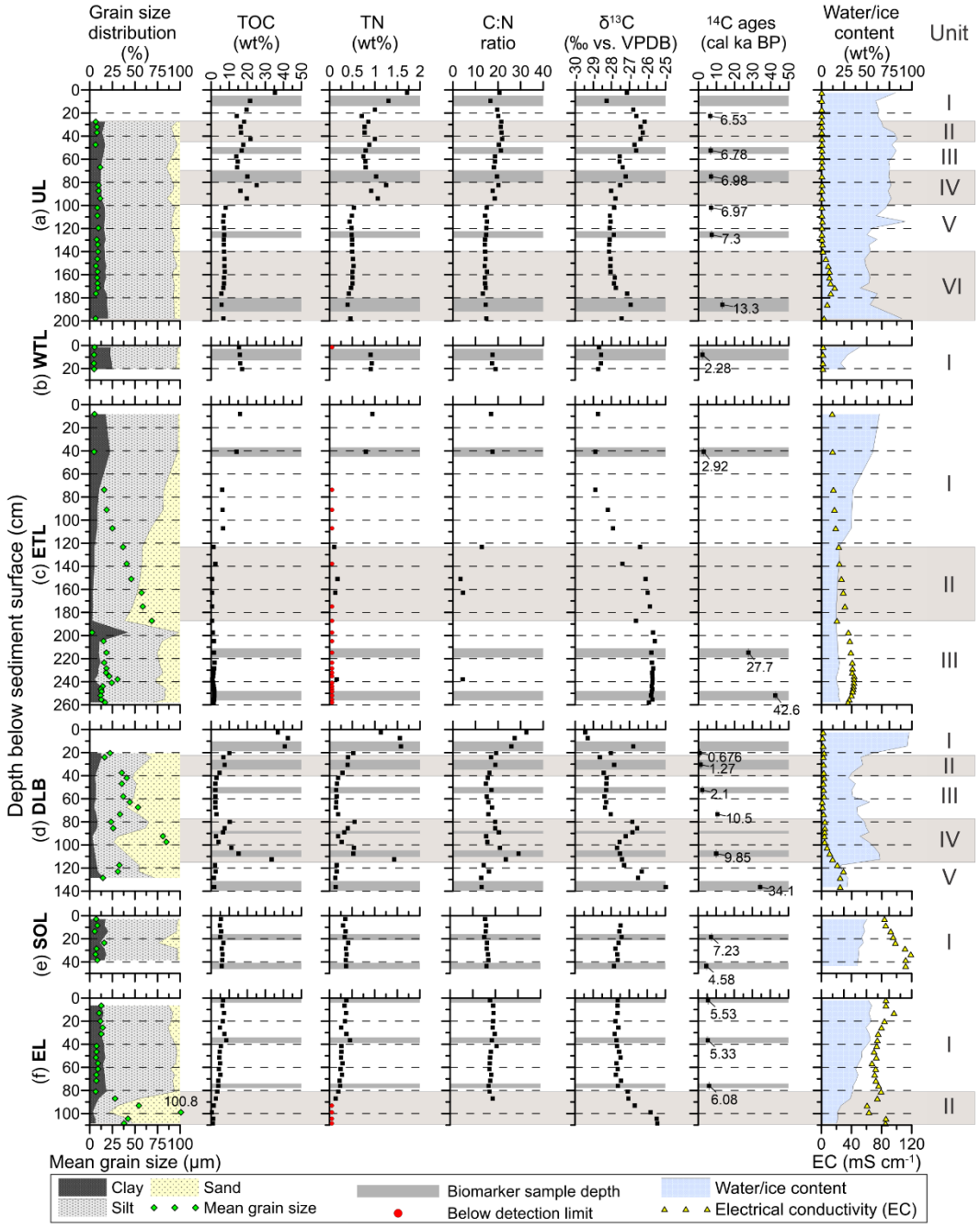

Figure 2: Sedimentological, elemental, isotopic and hydrochemical data from the investigated sediment cores: (a) UL (upland, 204 cm core length), (b) WTL (West Twin Lake, 23 cm core length), (c) ETL (East Twin Lake, 259 cm core length), (d) DLB (drained lake basin, 142 cm core length), (e) SOL (semi-open thermokarst lagoon, 46 cm core length), (f) EL (Elson Lagoon, 110 cm core length). Core units are based on parameter interpretation.

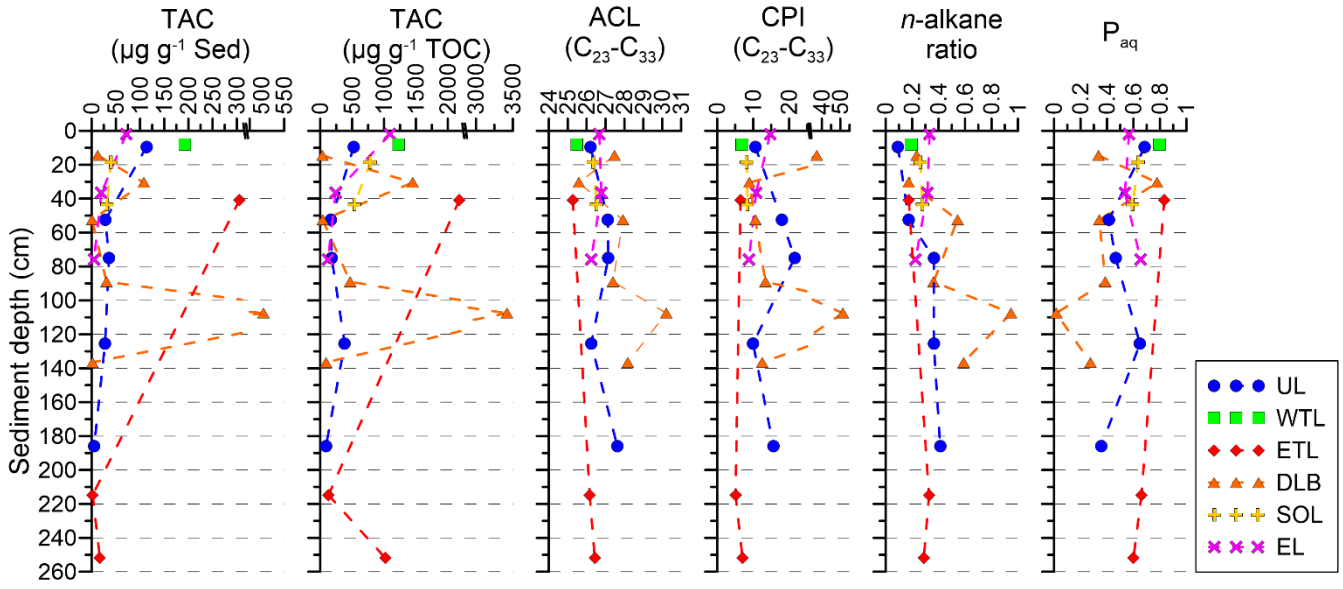

Figure 3: *n*-Alkane proxies along sediment cores: total *n*-alkane content (TAC) in µg g^{-1} sediment (Sed) and µg g^{-1} total organic carbon (TOC), average chain length (ACL), carbon preference index (CPI), *n*-alkane ratio and P_{aq}. The sediment cores comprise UL (upland, blue circle), WTL (West Twin Lake, green square), ETL (East Twin Lake, red diamond), DLB (drained lake basin, orange triangle), SOL (semi-open thermokarst lagoon, yellow plus), and EL (Elson Lagoon, magenta cross).

3.1.5 Semi-open thermokarst lagoon

The thermokarst lagoon core contains silty sediments (Fig. 2e). The average water content is 44.4±3.6 wt% and the porewater is characterized by hypersaline conditions with a peak value of 119.0 mS cm^{-1} at 34 cm depth. Radiocarbon dating of plant macrofossils shows an age-depth inversion with 7.2 cal ka BP at 19 cm depth and 4.6 cal ka BP at 44 cm depth. The TOC and TN contents average 5.8±0.6 wt% and 0.4±0.0 wt%, respectively. This results in an average C:N ratio of 16.1±0.6. Relatively homogenous values are also found for $\delta^{13}C$ with an average of -27.6±0.1 ‰. C:N and $\delta^{13}C$ ($r = -0.50$, $p = 0.17$) are not correlating (Fig. S1).

The two analyzed biomarker samples in the thermokarst lagoon are similar (Fig. 3). A TAC of 40.0 µg g^{-1} Sed (784.8 µg g^{-1} TOC) and 31.5 µg g^{-1} Sed (534.7 µg g^{-1} TOC) is present at 19 and 44 cm depth, respectively. The average ACL (26.4±0.1) and CPI (8.3±0.1) lie between the observed values of the thermokarst lakes and the terrestrial sites. Also, the terrestrial *n*-alkane ratio (average 0.3±0.0), and P_{aq} (average 0.6±0.0) are within the range of values observed in the other cores.

3.1.6 Elson Lagoon

The Elson Lagoon core comprises silty sediments underlain by sand (Fig. 2f). The maximum and minimum porewater contents are 55.8 and 16.6 wt% at 7 and 109 cm depth, respectively. Compared to the thermokarst lagoon, Elson Lagoon is less saline, yet hypersaline conditions prevail (on average 76.2±8.7 mS cm^{-1}). Radiocarbon ages signalize sediment mixing

as plant macrofossils have an age of 5.5 cal ka BP at 2 cm depth and 5.3 cal ka BP at 37 cm depth. Along the core, TOC contents are on average 4.5±2.2 wt% and show a decreasing trend. Until 87 cm depth, TN averages 0.3±0.1 wt%, and contents are < 0.1 wt% below this depth. The C:N ratio is relatively homogenous with an average of 18.4±0.9. $\delta^{13}C$ lies on average at -27.7±0.1 ‰ until 76 cm depth (Unit I). From 81 to 109 cm depth (Unit II) $\delta^{13}C$ precipitously increases to -25.4 ‰, which is the maximum value compared to all cores. No correlation is found between C:N and $\delta^{13}C$ ($r = -0.26$, $p = 0.32$; Fig. S1).

The sediments of Elson Lagoon reveal a decreasing trend of TAC with depth (average 32.1±28.5 µg g^{-1} Sed; 483.9±432.2 µg g^{-1} TOC; Fig. 3). *n*-Alkane proxies compare generally well to the thermokarst lagoon with the exception of the CPI. The degradation proxy indicates less degraded material (average 11.4±2.4) in the non-thermokarst lagoon compared to the thermokarst lagoon. Otherwise, the average ACL (26.6±0.2), terrestrial *n*-alkane ratio (0.3±0.0), and P_{aq} (0.6±0.0) are similar as in the thermokarst lagoon.

3.2 Influence of temperature and salinity

3.2.1 Thermal sediment stages

Our five thermal sediment stages comprise *seasonally frozen* including the max. active layer depths of the upland and the DLB after Nyland et al. (2021), perennially *frozen* referring to the permafrost domain of the upland, *unfrozen* (talik/cryopeg of West and East Twin Lake), *refrozen* corresponding to DLB permafrost and *lagoon* (thermokarst lagoon and Elson Lagoon) (for details see Table S9).

Kruskal-Wallis tests show that significant differences exist among the thermal regimes for TOC ($p < 0.001$), C:N ($p < 0.001$), and $\delta^{13}C$ ($p = 0.02$) (Table S9). Significance levels of pairwise Mann-Whitney test results are visualized in Fig. 4. The PERMANOVA test considering the combination of TOC, C:N and $\delta^{13}C$ indicated significant differences between thermal regimes ($r = 0.40$, $p = 0.001$). Post-hoc testing revealed that *unfrozen* sediments are significantly different from *frozen* ($r = 0.40$, $p = 0.05$), *refrozen* ($r = 0.55$, $p = 0.02$), and *lagoon* sediments ($r = 0.40$, $p = 0.04$). *Frozen* sediments further differ from *refrozen* ($r = 0.40$, $p = 0.03$) and *lagoon* ($r = 0.55$, $p = 0.01$) sediments. Also, significant differences exist between *refrozen* and *lagoon* sediments ($r= 0.40$, $p = 0.03$).

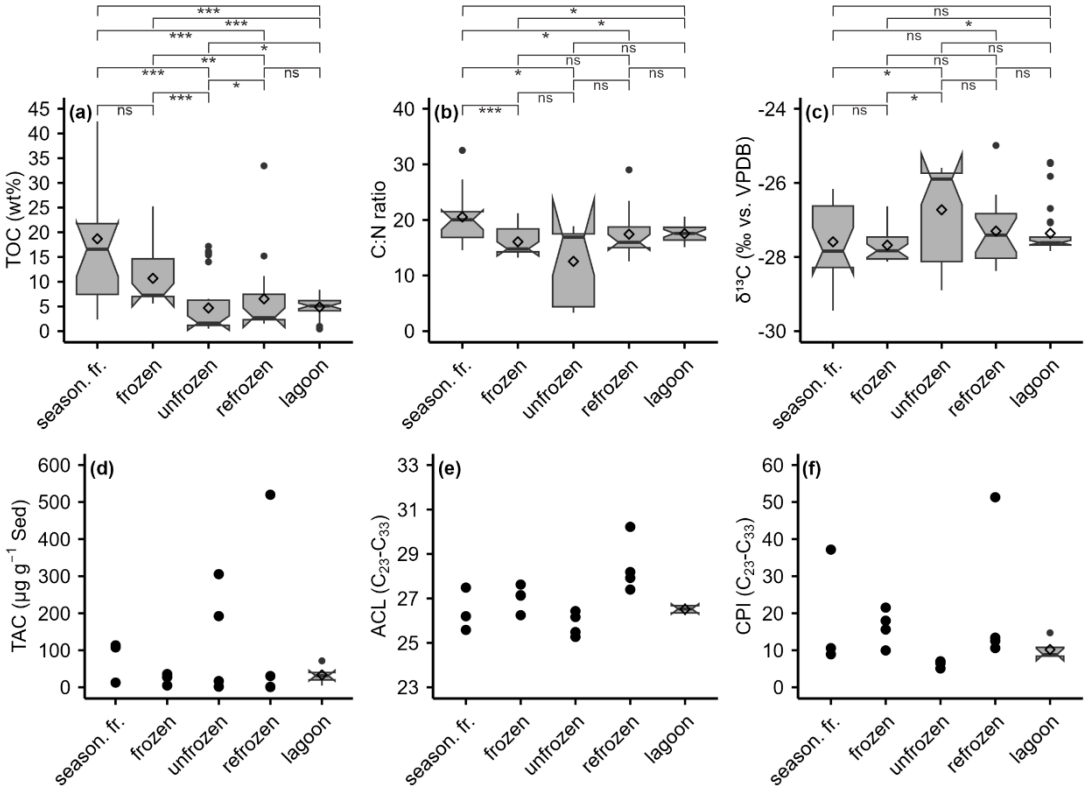

Figure 4: Notched boxplots of organic geochemical parameters across thermal regimes. Boxplots are shown for sample counts >4 and include medians (center lines), interquartile ranges (IQR, 25th-75th percentile), whiskers (1.5 × IQR), outliers (points), and means (diamonds). Notches display the 95 % confidence interval. Significance brackets in panel a-c comprise the significance levels p < 0.001 (***), p < 0.01 (**), p < 0.05 (*) and p > 0.05 (ns). Sediment classes comprise seasonally frozen (season. fr.), frozen, unfrozen, refrozen and lagoon.

3.2.2 Salinity stages

Grouping of sediment samples was conducted after previously defined salinity stages (section 2.2.2, for details see Table S10).

Significant differences in TOC ($p < 0.001$), C:N ($p < 0.001$), and $\delta^{13}C$ ($p < 0.001$) exist across at least some of the defined salinity stages according to Kruskal-Wallis (Table S10). Pairwise Mann-Whitney test significant levels are plotted in Fig. 5. PERMANOVA testing indicated that significant differences in salinity categories exist ($r = 0.55$, $p = 0.001$). Post-hoc testing revealed weak but significant differences between *brackish* and *hypersaline* samples ($r = 0.07$, $p = 0.05$).

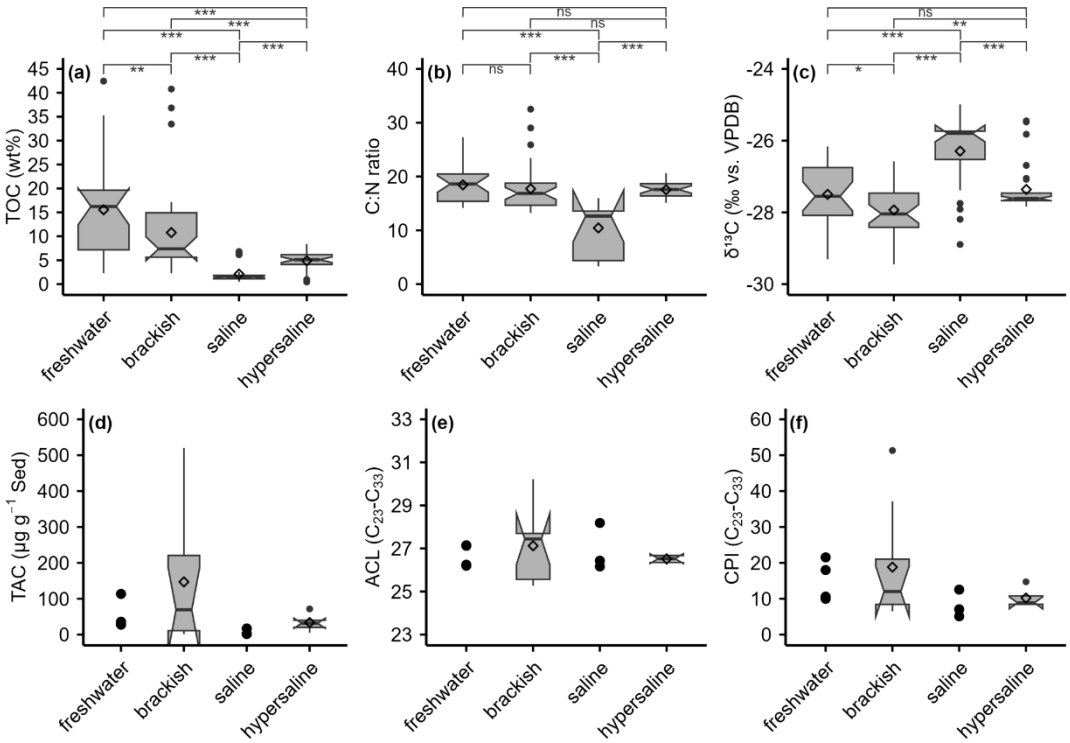

Figure 5: Notched boxplots of organic carbon parameters based on salinity categories (freshwater, >1.5 mS cm^{-1}; brackish, 1.5-15 mS cm^{-1}; saline, 15-50 mS cm^{-1}; hypersaline, >50 mS cm^{-1}). Boxplots are shown for sample counts > 4 and include medians (center lines), interquartile ranges (IQR, 25th-75th percentile), whiskers (1.5 × IQR), outliers (points), and means (diamonds). Notches display the 95 % confidence interval. Significance brackets are plotted for (a) TOC, (b) C:N, (c) δ13C and comprise the significance levels p < 0.001 (***), p < 0.01 (**), p < 0.05 (*), and p > 0.05 (ns).

3.2.3 Combined effect of thermal and salinity regimes

Since thermal and salinity stages were considered individually concerning their influence on organic matter characteristics, their combined impact was also investigated. Combining the thermal and salinity stages into unique groups resulted in eleven groups (Table 1). In PERMANOVA tests specific groups were excluded from the analysis due to low sample counts (n < 5 in G5, G7, G8, G10, Table 1). The PERMANOVA indicated that groups differ significantly from each other concerning TOC, C:N and $\delta^{13}C$ (r = 0.58, p = 0.001). Post-hoc pairwise PERMANOVA tests revealed that Group 2 and Group 6 were significantly different (r = 0.87, p = 0.03). Also, Group 3 differed significantly from Group 9 (r = 0.87, p < 0.01).

Table 1: Grouped thermal and salinity regimes and contributing cores. Sample count (*n*) in individual groups with reduced number after n/a removal in brackets (only samples with complete TOC, C:N, and $\delta^{13}C$ data were included in the statistical analyses). Asterisks mark small group sizes (< 5). These groups were not considered in the PERMANOVA analyses. UL - Upland, WTL - West Twin Lake, ETL - East Twin Lake, DLB - Drained lake basin, SOL - Semi-open thermokarst lagoon, EL - Elson Lagoon.

Group	Thermal regime	Salinity stage	Contributing core	*n*
G1	seasonally frozen	freshwater	UL, DLB	9

G2	seasonally frozen	brackish	DLB	8
G3	frozen	freshwater	UL	16
G4	frozen	brackish	UL	9
G5	frozen	saline	UL	1*
G6	unfrozen	brackish	WTL, ETL	6 (5)
G7	unfrozen	saline	ETL	24 (4)*
G8	refrozen	freshwater	DLB	2*
G9	refrozen	brackish	DLB	11
G10	refrozen	saline	DLB	4*
G11	lagoon	hypersaline	SOL, EL	31 (26)

4. Discussion

4.1 Modern and paleoenvironmental processes and conditions

The biogeochemistry of the investigated landforms provides insights into the landscape history and current environmental conditions.

4.1.1 Permafrost upland

The recent active layer depth in the tundra ranges between 29 cm and 47 cm (Nyland et al., 2021). This aligns well with the increased TOC and TN contents of Unit I (Fig. 2a). Measured electrical conductivity in the sediments reflects freshwater conditions, consistent with observations from the same upland (Jones et al., 2023) and in nearby streams (Lougheed et al., 2020). Unit II represents the range of the late-season thaw depth and the transient layer, which can be recognized by increased water/ice contents (Shur et al., 2005). The permafrost begins below 47 cm (Unit III). Bockheim et al., (1999) found that > 75 % of soils in the region are affected by cryoturbation; signs for this are found between 70 and 100 cm depths (Unit IV, Table S2). TOC and TN contents are increased compared to the units above and below, and the radiocarbon dates reveal an age-depth inversion. Cryoturbation at this depth could point towards a paleo active layer from the mid Holocene. Relatively homogenous conditions in the second meter (Unit V, VI) indicate fairly stable conditions from the Late Glacial into the early Holocene period.

Through the investigation of pollen records, Meyer et al. (2010) describe a shift from a purely grass dominated tundra in the Late Glacial towards a grass, sedge, and dwarf shrub mix in the early Holocene. Considering the terrestrial *n*-alkane proxies ACL and the *n*-alkane ratio, it could be inferred that this slowly occurring shrubification throughout the Holocene can be

confirmed by our *n*-alkane analysis due to the tendency towards lower ACL and *n*-alkane ratio values in Holocene samples compared to the deepest (Late Glacial) biomarker sample (Fig. 3). Furthermore, an aquatic influence indicated by the P_{aq} (section 3.3.1) may be explained by the presence of *Sphagnum* moss in ice-wedge troughs (Lara et al., 2015). However, P_{aq} could also be affected by mid-chain-length dominated *Betula* shrubs, whose *n*-alkane distributions can overlap with those of aquatic vegetation, limiting its source specificity (Ficken et al., 2000; Weber and Schwark, 2020).

4.1.2 Thermokarst lakes

Different from the gradual top-down thaw processes in the upland, thermokarst lakes are affected by abrupt thaw processes which can reach deeper deposits over short time scales (Grosse et al., 2011; Webb et al., 2025). While uplands and thermokarst lakes are sedimentologically connected due to the same parent material, the biogeochemical fingerprints of lakes may have changed due to recent thaw processes and lacustrine deposition. Comparing our two lake sites is challenging, as the West Twin Lake core is short, thus, a full comparison to the longer East Twin Lake core is somewhat limited. The main difference lies in the salinity between the lake sediments. While brackish conditions occur beneath West Twin Lake, the sediments of East Twin Lake have predominantly saline porewater (Fig. 2b, c). In East Twin Lake, electrical conductivity was observed to have almost tripled between 2016 and 2022 (Jones et al., 2023). As negative temperatures were measured in these sediments (Jones et al., 2023), we defined the unfrozen sediments as a cryopeg. Since brackish talik sediments were determined in the freshwater West Twin Lake, a near-future shift towards brackish lake water is likely. East Twin Lake's sediments (ca. 123 cm, Unit I) can be distinguished from the underlying late Pleistocene marine influenced sediments (Unit III) by considering the TOC contents (Eisner et al., 2005). These are in the range of values observed in the Teshepuk Lake area, ca. 120 km east of the Utqiaġvik Peninsula (Lenz et al., 2016). P_{aq} indicates an increased aquatic influence in the upper sediments. Yet ACL and the *n*-alkane ratio also indicate terrestrial plant input into the lake which can be explained by enhanced lateral expansion (shoreline erosion) in recent years (Jones et al., 2023). It needs to be stressed that in our study the ACL decreases with decreasing CPI values ($r = 0.79$, $p < 0.001$), meaning that the vegetation signal is influenced by organic matter degradation (strongest in East Twin Lake).

The transition from Unit II to III in the East Twin Lake core is characterized by a sharp decrease of the mean grain size from fine sand to silt. The sand might be aeolian which deposited in the surface depression (Carter, 1981; Eisner et al., 2005). In both units, the C:N and $\delta^{13}C$ ratios point towards a marine/lacustrine algae production (Fig. 4b, c; Meyers, 1994), which aligns with the high salinity (Figure 2c). This pattern matches with the investigation of Meyer et al. (2010), who observed more enriched $\delta^{13}C$ values in the salty late Pleistocene sediments at a permafrost tunnel on the Utqiaġvik Peninsula.

4.1.3 Drained lake basin

In view of the landscape alteration, the next step is the drainage of thermokarst lakes where permafrost is re-forming. The DLB core revealed mixed signals. Electrical conductivity is similar to the upland, which is linked to Holocene ages, whereas the sediments are sandier, comparable to the East Twin Lake sediments. Brown et al. (2003) estimated that the lake drained

about 100-150 years ago; however, our radiocarbon dating revealed that post-drainage peat formation was initiated ca. 700 cal a BP (Fig. 2d). DLBs sequester organic carbon in the form of peat (Bockheim et al., 2004; Hinkel et al., 2003; Jones et al., 2012), which can be recognized by the highest TOC contents and C:N ratios in the upper 15 cm (Unit I). We argue that the most recent lake phase in the DLB started 1.3 cal ka BP and therefore lasted only approximately 600 years when considering the TOC contents (Unit II). Between 21 and 31 cm depth, TOC contents are in the range of contents found in the East Twin Lake sediments, and P_{aq} signalizes aquatic conditions. Our observation of the former lake phase shows that these periods are in this case shorter than previously estimated by Fuchs et al. (2019), who found that lakes persist a minimum of 1000 years in northern Alaska. The relatively carbon-poor and alkane-depleted sediments beneath the lake phase might be a refrozen talik starting beneath the modern active layer (Unit III). The brackish and refrozen sediments differed statistically from frozen upland deposits affected by freshwater conditions (Section 3.2.3). In Unit IV, increased TOC contents and a high *n*-alkane ratio - indicating the presence of herbaceous plants (Schäfer et al., 2016) - point toward one or even two wetland periods with organic matter accumulation, which likely occurred during the Holocene Thermal Maximum (Jones and Yu, 2010; Kaufman et al., 2004). The low TOC and TN content at 93 cm depth make it difficult to clarify whether a first wetland period was followed by another, as this impression could also result from cryoturbation. The age-depth inversion is an indication of both a refrozen talik and intensified freeze-thaw dynamics during the early Holocene. Unit V represents the late Pleistocene to early Holocene transition as indicated by the trend towards more negative $\delta^{13}C$ values (Fig. 2d).

4.1.4 Lagoons

If thermokarst lakes or their drained basins are connected and inundated by sea water, they become thermokarst lagoons. With a size of 80 ha, the semi-open thermokarst lagoon is a relatively small lagoon based on the circum-Arctic thermokarst lagoon assessment published by Jenrich et al. (2025b). TOC contents are higher compared to other lagoons, such as on the Bykovsky Peninsula in Siberia (Jenrich et al., 2021; Schirrmeister et al., 2018; Ulyantsev et al., 2017; Yang et al., 2023), in northwestern Canada (Jenrich et al., 2025a), and the Teshepuk Lake area (Giest et al., 2025). Shoreline erosion and fluvial organic matter input from streams (Fig. 1) are likely driving factors for this pattern.

Elson Lagoon, which is not a thermokarst lagoon, receives terrestrial sediment input through coastal erosion, and deposition takes place as the barrier islands protect the waters of the lagoon (Brown et al., 2003; Ping et al., 2011; Zimmermann et al., 2022). Our investigations indicate that the upper 80 cm of the sediments are terrestrial deposits, since the biogeochemical parameters are overall very similar to the values found in the sediments of the thermokarst lagoon (Unit I; Fig. 2f, 3). These are underlain by likely late Pleistocene to early Holocene sandy sediments (Unit II).

The age-depth inversions signalize sediment mixing in both lagoons, which is favored through the semi- to unfrozen conditions (Table S1). The hypersalinity in the sediments might be the result from concentrating salt through bedfasting ice in the shallow lagoons (Jenrich et al., 2021). Hypersaline conditions in Elson Lagoon were quantified earlier by Osterkamp and Harrison (1985) as well as Overduin et al. (2012).

4.2 Organic matter degradation patterns

For the terrestrial sampling measurements in the permafrost upland, the average C:N ratio (17.1±2.1) compares well to values reported in similar sites in northern Alaska (Fuchs et al., 2019; Giest et al., 2025; Ping et al., 2011). The comparably lower ratio in the second meter (Unit V, VI) points towards a slightly higher degradation state (Fig. 2a). C:N ratios are lower compared to permafrost-affected peat (20-60; Andersson et al., 2012) but similar or higher than in Yedoma deposits (9-19; Strauss et al., 2022). Since $\delta^{13}C$ values become less negative with degradation, C:N should correlate negatively with $\delta^{13}C$ (Strauss et al., 2015). In our upland core however, this relationship shows a significant positive correlation (Fig. S1). Since the CPI shows mixed but high (> 10) values, we can conclude that organic matter is overall relatively well preserved in the upland. PERMANOVA test results indicated that *frozen* sediments are distinct from sediments affected by thaw processes, namely *unfrozen*, *refrozen* and *lagoon* sediments. This expresses the possibility of statistically distinguishing between sediments of various thaw histories.

For the first degradation stage with the subaquatic talik/cryopeg phase, PERMANOVA testing also revealed a distinct biochemical signal of *unfrozen* sediments when compared to *frozen*, *refrozen*, and *lagoon* sediments. This result, as for the upland, is likely influenced by source signals, especially when terrestrial and marine deposits are compared. But since the CPI in the lakes is comparably lower than in the upland and the DLB, the organic matter generally seems to be more degraded in the thermokarst lakes (Fig. 3). Moreover, the CPI in the saline East Twin Lake sediments expressed signs for stronger degradation (6.2) than in the brackish West Twin Lake sediments (6.9). This might result from degradation under unfrozen cryotic, and saline conditions (Li et al., 2024). Compared to Yedoma and other thermokarst lake sediments, the CPI values indicate a similar degree of organic matter decomposition (Jongejans et al., 2020) or even stronger decomposition (Jongejans et al., 2021).

For the DLB, the carbon quality shows fresh organic matter in the surface peat (Unit I) which, together with the surface sediments of the upland, makes *seasonally frozen* organic-rich sediments distinguishable from all other thermal regimes considering C:N as shown by the Mann-Whitney tests (Fig. 4b). This is followed by more degraded conditions in the refrozen talik (Unit II, III) and well-preserved organic matter in the former wetland phase (Unit IV). The C:N ratio and the CPI index agree in their patterns; however, $\delta^{13}C$ only poorly reflects this picture (Fig. 2d, 3). Therefore, C:N and $\delta^{13}C$ resulted in a weak and non-significant correlation. Especially the peak $\delta^{13}C$ values (least negative) in Unit I and IV disturb the relationship, and it is likely that the source (i.e., lacustrine) signal of the isotopes is responsible for this pattern. Based on C:N and CPI, Unit V indicates comparably stronger degraded organic matter, combined with a marine $\delta^{13}C$ signal (maximum -25.0 ‰). The unique pattern of refrozen sediments is reflected in the PERMANOVA results as the *refrozen* sediments could be differentiated from *frozen* and *unfrozen* terrestrial sediments as well as *lagoon* deposits. Our DLB surface C:N and $\delta^{13}C$ values fit into the range observed by Wolter et al. (2024). Comparing the average C:N of the full core (18.6) to other study areas in northern Alaska and northwest Canada however indicates less degraded conditions than observed by

Giest et al. (2025) (17.5), Fuchs et al. (2019) (16.6) and Wolter et al. (2017) (13.2). The increased C:N ratios from Unit IV are pivotal reasons for this result, as early wetland phases were not described in the aforementioned studies.

For the lagoons, the organic matter degradation proxies reflect relatively little variability within the sediments and represent a mixed signal from the terrestrial and lacustrine sites (Fig. 2, 3, 4). Although individual statistical tests of hypersaline lagoon sediments revealed differences to other sediment types (section 3.2.1 and 3.2.2), the combined effect of thermal and salinity regimes in lagoon sediments did not differ significantly from other sediment types (section 3.2.3). The reasons for this are the various sediment types that are mixed in the investigated lagoons. The C:N ratio and CPI indicate relatively stronger degraded material in the semi-open thermokarst lagoon compared to Elson Lagoon, though compared to lagoons in northern Alaska and Siberia, both exhibit well-preserved organic matter, which can be explained by their terrestrial origin (Giest et al., 2025; Jenrich et al., 2021; Schirrmeister et al., 2018; Yang et al., 2023).

4.3 Implications and outlook

Our biogeochemical investigations into representative landforms of northernmost coastal Alaska provide a valuable basis for evaluating potential implications and future developments of the region. Based on this, we drew a conceptual model of landscape dynamics in the study area (Fig. 6).

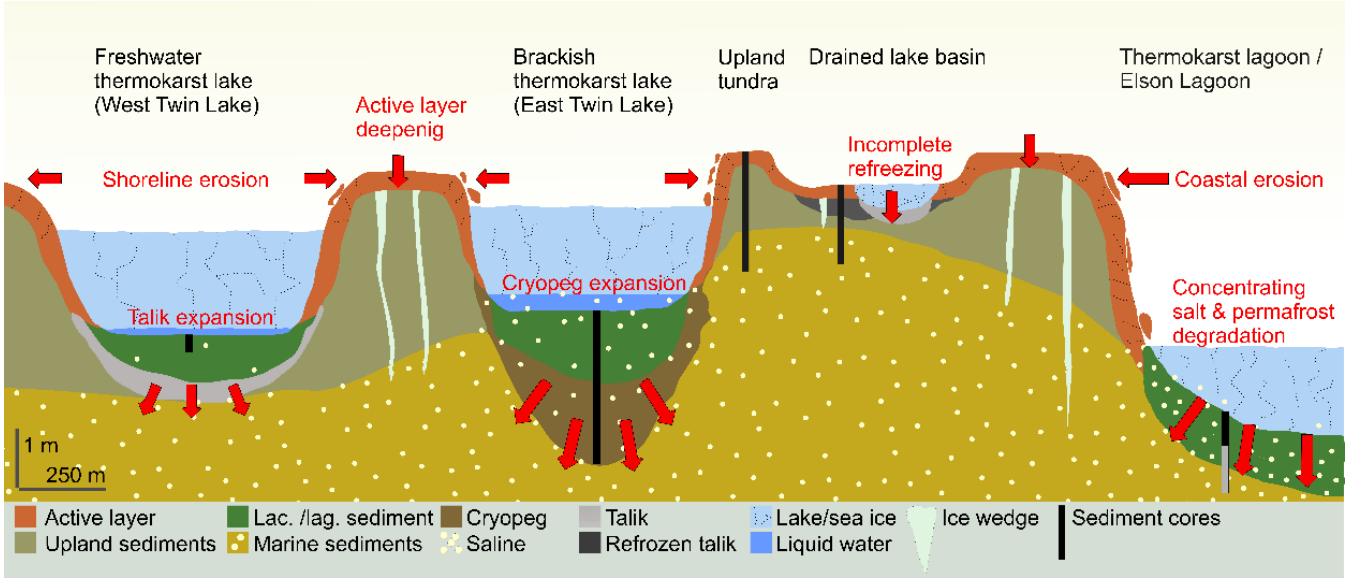

Figure 6: Conceptual illustration of physical properties and dynamics currently affecting the Utqiaġvik Peninsula with potential for future acceleration. The sediments are present in a variety of thermal states, seasonally frozen (active layer), perennially frozen (upland tundra and subsea marine sediments), unfrozen (talik, lacustrine sediments, partly in the drained lake basin), unfrozen cryotic (cryopeg and lacustrine/lagoon sediments) and refrozen (drained lake basin). Model illustrated at approximate scale.

Remnant permafrost uplands cover ca. 28 % of today's landscape in the study area (Hinkel et al., 2005; Jones et al., 2022) where saline permafrost underlays Holocene deposits (Brigham-Grette and Hopkins, 1995; Brouchkov, 2003; Eisner et al., 2005). These non-saline sediments have a thickness of less than 1.5 m in our investigated upland. Increasing active layer

depths in the tundra, with widespread thickening across >80 % of northern permafrost regions since 2003 (Liu et al., 2024; Smith et al., 2022) cause the mobilization and (dominantly) aerobic mineralization of organic carbon, leading to CO_2 production (Jenrich et al., 2024). Once thaw reaches to depths of the saline deposits, degradation processes will be enhanced as the freezing point is depressed. This poses the risk that subaerial taliks and cryopegs will be initiated earlier than the 22nd century as hitherto projected by Parazoo et al. (2018).

East Twin Lake has already undergone this development turning it from a freshwater to a brackish/saline thermokarst lake, which led to increased thermoerosion rates (Jones et al., 2023). Brown et al. (2003) calculated that the lake will likely drain into Elson Lagoon (or turn into a thermokarst lagoon) by the 2040s. However, this estimate was purely based on lake and lagoonal shoreline erosion rates while other processes, such as sea level rise, widespread gradual thaw with continued warming and rapid saline permafrost degradation were not accounted for (Creel et al., 2024; Guimond et al., 2021; Jones et al., 2023). These processes further increase the forcing, potentially leading to faster-than-anticipated landscape changes. The timing of a potential future drainage event of West Twin Lake is more difficult to estimate, but the drainage pathway may be via the thermoerosional gully to the south of the lake (Fig. 1). A supra-permafrost groundwater connection between the lake and Elson Lagoon may also play a (future) role in groundwater discharge (Dimova et al., 2015; Rawlins, 2021), yet Guimond et al. (2022) conclude that groundwater is not a significant factor at the north Alaskan coast due to a low land to sea hydraulic gradient. The talik beneath West Twin Lake has already reached brackish deposits, and with continued thaw beneath the lake, it can be expected that the lake's water will turn brackish in the near future, too. This in turn would have implications for lake ice dynamics and continued thaw beneath the lake. Arp et al. (2012) observed a trend from bedfast towards floating lake ice conditions in northernmost Alaska, but the impact of saline conditions was not accounted for. Considering the vulnerability of permafrost to salt, it can be expected that the aforementioned cascading effects of salt intrusion into lake waters will play a crucial role across the Younger Outer Coastal Plain, as exemplified by East Twin Lake which has regionally representative lake morphometrics (Table S1; Arp et al., 2011; Jones et al., 2023). The organic deposits within both lake's sediments are already relatively stronger degraded than in the upland, and organic matter of the cryopeg in East Twin Lake is more heavily degraded than in the West Twin Lake talik. From a microbiological point of view, this can be explained by microbial communities that are likely dominated by methanogens (CH_4 producers) in West Twin Lake while in East Twin Lake sulfate-reducing microbes (CO_2 producers) probably established additionally due to the saline deposits (Jenrich et al., 2024; Yang et al., 2023). A potential co-existence of these microbial communities may lead to enhanced greenhouse gas production. This comparison stresses the potential for year-round salinity influenced organic carbon mineralization at sub-zero temperatures.

Northernmost Alaska is a highly dynamic region which is experiencing a net thermokarst lake area loss trend mostly due to drainage of large lakes (Nitze et al., 2017; Webb et al., 2022). A detailed analysis of pond dynamics within DLBs on the Utqiaġvik Peninsula could also verify a drainage trend (Andresen and Lougheed, 2015). We investigated a wet but terrestrial site within the DLB with a refrozen talik. Still, two larger thermokarst ponds are situated nearby with potential taliks beneath. Thus, although the basin sequesters peat, it can be expected that organic matter degradation also takes place locally.

Especially the former wetland phase (Unit IV, Fig. 2d, 3) indicates well preserved organics in the sediment, holding a high potential for degradation. If these ponds drain, it can be expected that permafrost aggradation will progressively slow with continued climate warming and freezing point depression in saline deposits (Jones et al., 2022; Lantz et al., 2022). Moreover, Wolter et al. (2024) quantified high CH_4 concentrations in submerged areas within DLBs showcasing the potential for carbon mineralization under current environmental and climatic conditions.

When terrestrial or lacustrine deposits transition into, or are eroded into, lagoon systems, thawed organic matter becomes vulnerable to decomposition under now hypersaline conditions. We found that the lagoonal deposits represent a mixed signal of the terrestrial and lacustrine sediments rather than further advanced degradation. With increasing marine influence, it can be expected that greenhouse gas production shifts from mixed CH_4 and CO_2 in low connected water bodies (such as the semi-open thermokarst lagoon) towards pure CO_2 production in more marine settings (like Elson Lagoon, Jenrich et al., 2025a). Submarine permafrost degradation rates of up to 4 cm yr^{-1} in Elson Lagoon (Overduin et al., 2012) also contribute to enlarging the carbon pool availability for mineralization. The high carbon content and the relatively well-preserved organic matter therefore exhibits a large potential for future carbon mineralization in lagoon systems.

Overall, observed carbon and landscape dynamics can be expected to play a major role across the wider saline permafrost region. Brouchkov (2003) published an estimated map of the saline permafrost zone, however large-scale quantifications of the saline permafrost distribution and its properties, including organic carbon stocks, are currently lacking. This calls for future study efforts, which would constitute important steps forward in understanding the role of salt in Arctic permafrost.

5. Conclusions

Our study reveals distinct patterns of organic matter alteration along gradients of thaw and salinity stages on the Arctic Coastal Plain of Alaska.

Regarding research question 1, which addressed how paleoenvironmental and modern processes shape present-day sediment characteristics on the Utqiaġvik Peninsula, we found that late Pleistocene saline deposits are overlain by less than 1.5 m organic-rich, well-preserved sediments from an early Holocene wetland phase and a mid-Holocene active layer, as observed in the DLB and the remnant permafrost upland, respectively. Thermokarst lake subsidence has transformed these landscapes, with West Twin Lake reaching brackish sediment conditions and East Twin Lake progressing towards brackish/saline states. Biogeochemical signatures indicate ongoing input of terrestrial and lacustrine sediments into the lagoons.

In response to research question 2, which focused on organic matter quality in thermokarst landforms, we conclude that organic matter degradation is enhanced in the brackish talik of West Twin Lake and particularly in the cryopeg of East Twin Lake. Lagoonal sediments show a high potential for carbon mineralization, driven by salt accumulation beneath bedfast ice that has created hypersaline conditions. These conditions have maintained year-round unfrozen zones, enabling microbial activity and greenhouse gas production.

Concerning research question 3, which asked how landscape dynamics affect organic matter mobilization, we anticipate that deepening active layers, the formation of taliks and cryopegs, and ongoing shoreline erosion in lakes and lagoons will

increase the risk of organic carbon mobilization and mineralization. This risk is especially pronounced in saline deposits and may accelerate landscape change across the saline permafrost region, with substantial implications for permafrost carbon release.

Our findings show a need for additional local investigations and upscaling efforts assessing the consequences of saline permafrost thaw. While focused on a specific site on the northernmost tip of the USA, our study captures processes and conditions that are likely characteristic of extensive saline permafrost landscapes across the Arctic, underscoring its significance for regional-scale assessments of carbon dynamics.

Data availability

The data used for this study is available in the PANGAEA open access archive under: https://doi.pangaea.de/10.1594/PANGAEA.983965 (biogeochemical and hydrochemical data) and https://doi.pangaea.de/10.1594/PANGAEA.983966 (*n*-alkane data).

Author Contributions

FS and JS designed the study. JS, GG, MJ, and BMJ conducted fieldwork. FS, MJ, and JS carried out sediment subsampling. FS conducted laboratory work, analyzed and plotted data, and wrote the first manuscript. All authors contributed to the development of the paper.

Competing interests

Some authors are members of the editorial board of EGU Biogeosciences.

Acknowledgements

The SIPRE corer for this work was gratefully provided by Kenneth M. Hinkel (University of Cincinnati) and the vibracorer was gratefully provided by Chris Mayo (University of Alaska Fairbanks). We also thank the Ukpeaġvik Iñupiat Corporation (UIC) for issuing the permit for this research and providing logistical support. We would like to thank Lars Ebel and the AWI laboratories Permafrost Biogeochemistry, Permafrost Hydrochemistry, ISOLAB and MICADAS for their support. Finally, we would like to thank the anonymous reviewers and the associate editor for their valuable comments. This work is a contribution to the IPA Saline Permafrost Action Group.

Financial support

FS and MJ received funding from the German Federal Environmental Foundation (Deutsche Bundesstiftung Umwelt). Fieldwork was supported by NSF Office of Polar Program awards (1806213, 2336164) and AWI expedition baseline funding. The authors acknowledge support by the Open Access publication fund of Alfred Wegener Institute Helmholtz Centre for Polar and Marine Research

References

Alewell, C., Giesler, R., Klaminder, J., Leifeld, J., and Rollog, M.: Stable carbon isotopes as indicators for environmental change in palsa peats, Biogeosciences, 8, 1769–1778, https://doi.org/10.5194/bg-8-1769-2011, 2011.

Andersson, R. A. and Meyers, P. A.: Effect of climate change on delivery and degradation of lipid biomarkers in a Holocene peat sequence in the Eastern European Russian Arctic, Organic Geochemistry, 53, 63–72, https://doi.org/10.1016/j.orggeochem.2012.05.002, 2012.

Andersson, R. A., Meyers, P., Hornibrook, E., Kuhry, P., and Mörth, C.-M.: Elemental and isotopic carbon and nitrogen records of organic matter accumulation in a Holocene permafrost peat sequence in the East European Russian Arctic, Journal of Quaternary Science, 27, 545–552, https://doi.org/10.1002/jqs.2541, 2012.

Andresen, C. G. and Lougheed, V. L.: Disappearing Arctic tundra ponds: Fine-scale analysis of surface hydrology in drained thaw lake basins over a 65 year period (1948-2013), J. Geophys. Res. Biogeosci., 120, 466–479, https://doi.org/10.1002/2014JG002778, 2015.

Arp, C. D., Jones, B. M., Schmutz, J. A., Urban, F. E., and Jorgenson, M. T.: Two mechanisms of aquatic and terrestrial habitat change along an Alaskan Arctic coastline, Polar Biol, 33, 1629–1640, https://doi.org/10.1007/s00300-010-0800-5, 2010.

Arp, C. D., Jones, B. M., Urban, F. E., and Grosse, G.: Hydrogeomorphic processes of thermokarst lakes with grounded-ice and floating-ice regimes on the Arctic coastal plain, Alaska, Hydrological Processes, 25, 2422–2438, https://doi.org/10.1002/hyp.8019, 2011.

Arp, C. D., Jones, B. M., Lu, Z., and Whitman, M. S.: Shifting balance of thermokarst lake ice regimes across the Arctic Coastal Plain of northern Alaska, Geophysical Research Letters, 39, https://doi.org/10.1029/2012GL052518, 2012.

Athy, L. F.: Density, Porosity, and Compaction of Sedimentary Rocks1, AAPG Bulletin, 14, 1–24, https://doi.org/10.1306/3D93289E-16B1-11D7-8645000102C1865D, 1930.

Baas, M., Pancost, R., van Geel, B., and Sinninghe Damsté, J. S.: A comparative study of lipids in Sphagnum species, Organic Geochemistry, 31, 535–541, https://doi.org/10.1016/S0146-6380(00)00037-1, 2000.

Biskaborn, B. K., Smith, S. L., Noetzli, J., Matthes, H., Vieira, G., Streletskiy, D. A., Schoeneich, P., Romanovsky, V. E., Lewkowicz, A. G., Abramov, A., Allard, M., Boike, J., Cable, W. L., Christiansen, H. H., Delaloye, R., Diekmann, B., Drozdov, D., Etzelmüller, B., Grosse, G., Guglielmin, M., Ingeman-Nielsen, T., Isaksen, K., Ishikawa, M., Johansson, M., Johannsson, H., Joo, A., Kaverin, D., Kholodov, A., Konstantinov, P., Kröger, T., Lambiel, C., Lanckman, J.-P., Luo, D., Malkova, G., Meiklejohn, I., Moskalenko, N., Oliva, M., Phillips, M., Ramos, M., Sannel, A. B. K., Sergeev, D., Seybold,

C., Skryabin, P., Vasiliev, A., Wu, Q., Yoshikawa, K., Zheleznyak, M., and Lantuit, H.: Permafrost is warming at a global scale, Nat Commun, 10, 264, https://doi.org/10.1038/s41467-018-08240-4, 2019.

Black, R. F.: Gubik Formation of Quaternary Age in Northern Alaska, 302nd–C ed., U.S. Government Printing Office, 59–91 pp., 1964.

Blott, S. J. and Pye, K.: GRADISTAT: a grain size distribution and statistics package for the analysis of unconsolidated sediments, Earth Surface Processes and Landforms, 26, 1237–1248, https://doi.org/10.1002/esp.261, 2001.

Bockheim, J. G., Everett, L. R., Hinkel, K. M., Nelson, F. E., and Brown, J.: Soil Organic Carbon Storage and Distribution in Arctic Tundra, Barrow, Alaska, Soil Science Society of America Journal, 63, 934–940, https://doi.org/10.2136/sssaj1999.634934x, 1999.

Bockheim, J. G., Hinkel, K. M., Eisner, W. R., and Dai, X. Y.: Carbon Pools and Accumulation Rates in an Age-Series of Soils in Drained Thaw-Lake Basins, Arctic Alaska, Soil Science Society of America Journal, 68, 697–704, https://doi.org/10.2136/sssaj2004.6970, 2004.

Bray, E. E. and Evans, E. D.: Hydrocarbons in Non-Reservoir-Rock Source Beds, AAPG Bulletin, 49, 248–257, 1965.

Brigham-Grette, J. and Hopkins, D. M.: Emergent Marine Record and Paleoclimate of the Last Interglaciation along the Northwest Alaskan Coast, Quaternary Research, 43, 159–173, https://doi.org/10.1006/qres.1995.1017, 1995.

Brittingham, A., Hren, M. T., and Hartman, G.: Microbial alteration of the hydrogen and carbon isotopic composition of n-alkanes in sediments, Organic Geochemistry, 107, 1–8, https://doi.org/10.1016/j.orggeochem.2017.01.010, 2017.

Brouchkov, A.: Nature and distribution of frozen saline sediments on the Russian Arctic coast, Permafrost and Periglacial Processes, 13, 83–90, https://doi.org/10.1002/ppp.411, 2002.

Brouchkov, A.: Frozen saline soils of the Arctic coast: their distribution and engineering properties, Proceedings of the eighth international conference on permafrost, 95–100, 2003.

Brown, J., Jorgenson, M. T., Smith, O. P., and Lee, W.: Long-term rates of coastal erosion and carbon input, Elson Lagoon, Barrow, Alaska, Proceedings of the 8th International Conference on Permafrost, 101–106, 2003.

Cahyadi, A., Fatchurohman, H., and Riyanto, I. A.: Groundwater quality analysis in dry seasons in Panggang Cay, Kepulauan Seribu, Jakarta, Indonesia, IOP Conf. Ser.: Earth Environ. Sci., 212, 012001, https://doi.org/10.1088/1755-1315/212/1/012001, 2018.

Carter, L. D.: A Pleistocene Sand Sea on the Alaskan Arctic Coastal Plain, Science, 211, 381–383, https://doi.org/10.1126/science.211.4480.381, 1981.

Chen, Y., Lara, M. J., Jones, B. M., Frost, G. V., and Hu, F. S.: Thermokarst acceleration in Arctic tundra driven by climate change and fire disturbance, One Earth, 4, 1718–1729, https://doi.org/10.1016/j.oneear.2021.11.011, 2021.

Chylek, P., Folland, C., Klett, J. D., Wang, M., Hengartner, N., Lesins, G., and Dubey, M. K.: Annual Mean Arctic Amplification 1970–2020: Observed and Simulated by CMIP6 Climate Models, Geophysical Research Letters, 49, e2022GL099371, https://doi.org/10.1029/2022GL099371, 2022.

Copernicus: Copernicus Sentinel-2 (processed by ESA), MSI Level-2A BOA Reflectance Product. Collection 0. European Space Agency, https://doi.org/https://doi.org/10.5270/S2_-6eb6imz, 2023.

Coplen, T. B., Brand, W. A., Gehre, M., Gröning, M., Meijer, H. A. J., Toman, B., and Verkouteren, R. M.: New Guidelines for δ13C Measurements, Anal. Chem., 78, 2439–2441, https://doi.org/10.1021/ac052027c, 2006.

Creel, R., Guimond, J., Jones, B. M., Nielsen, D. M., Bristol, E., Tweedie, C. E., and Overduin, P. P.: Permafrost thaw subsidence, sea-level rise, and erosion are transforming Alaska's Arctic coastal zone, Proceedings of the National Academy of Sciences, 121, e2409411121, https://doi.org/10.1073/pnas.2409411121, 2024.

DGGS: DGGS Elevation Portal, 2018.

Diefendorf, A. F., Freeman, K. H., Wing, S. L., and Graham, H. V.: Production of n-alkyl lipids in living plants and implications for the geologic past, Geochimica et Cosmochimica Acta, 75, 7472–7485, https://doi.org/10.1016/j.gca.2011.09.028, 2011.

Dimova, N. T., Paytan, A., Kessler, J. D., Sparrow, K. J., Garcia-Tigreros Kodovska, F., Lecher, A. L., Murray, J., and Tulaczyk, S. M.: Current Magnitude and Mechanisms of Groundwater Discharge in the Arctic: Case Study from Alaska, Environ. Sci. Technol., 49, 12036–12043, https://doi.org/10.1021/acs.est.5b02215, 2015.

Eglinton, G., Hamilton, R. J., Raphael, R. A., and Gonzalez, A. G.: Hydrocarbon Constituents of the Wax Coatings of Plant Leaves: A Taxonomic Survey, Nature, 193, 739–742, https://doi.org/10.1038/193739a0, 1962.

Eisner, W. R., Bockheim, J. G., Hinkel, K. M., Brown, T. A., Nelson, F. E., Peterson, K. M., and Jones, B. M.: Paleoenvironmental analyses of an organic deposit from an erosional landscape remnant, Arctic Coastal Plain of Alaska, Palaeogeography, Palaeoclimatology, Palaeoecology, 217, 187–204, https://doi.org/10.1016/j.palaeo.2004.11.025, 2005.

van Everdingen, R. O. (Ed.): Multi-language Glossary of Permafrost and Related Ground-ice Terms in Chinese, English, French, German, Icelandic, Italian, Norwegian, Polish, Romanian, Spanish, and Swedish, Arctic Inst. of North America University of Calgary, Calgary, Alberta, Canada, 2005.

Farquharson, L. M., Romanovsky, V. E., Kholodov, A., and Nicolsky, D.: Sub-aerial talik formation observed across the discontinuous permafrost zone of Alaska, Nat. Geosci., https://doi.org/10.1038/s41561-022-00952-z, 2022.

Ficken, K. J., Li, B., Swain, D. L., and Eglinton, G.: An n-alkane proxy for the sedimentary input of submerged/floating freshwater aquatic macrophytes, Organic Geochemistry, 31, 745–749, https://doi.org/10.1016/S0146-6380(00)00081-4, 2000.

Fuchs, M., Lenz, J., Jock, S., Nitze, I., Jones, B. M., Strauss, J., Günther, F., and Grosse, G.: Organic Carbon and Nitrogen Stocks Along a Thermokarst Lake Sequence in Arctic Alaska, Journal of Geophysical Research: Biogeosciences, 124, 1230–1247, https://doi.org/10.1029/2018JG004591, 2019.

Gibbs, A. E. and Richmond, B. M.: National assessment of shoreline change—Summary statistics for updated vector shorelines and associated shoreline change data for the north coast of Alaska, U.S.- Canadian border to Icy Cape, U.S. Geological Survey, Virginia, US, 2017.

Giest, F. P., Jenrich, M., Grosse, G., Jones, B. M., Mangelsdorf, K., Windirsch, T., and Strauss, J.: Organic carbon, mercury, and sediment characteristics along a land–shore transect in Arctic Alaska, Biogeosciences, 22, 2871–2887, https://doi.org/10.5194/bg-22-2871-2025, 2025.

Goñi, M. A., Yunker, M. B., Macdonald, R. W., and Eglinton, T. I.: Distribution and sources of organic biomarkers in arctic sediments from the Mackenzie River and Beaufort Shelf, Marine Chemistry, 71, 23–51, https://doi.org/10.1016/S0304-4203(00)00037-2, 2000.

Grosse, G., Harden, J., Turetsky, M., McGuire, A. D., Camill, P., Tarnocai, C., Frolking, S., Schuur, E. A. G., Jorgenson, T., Marchenko, S., Romanovsky, V., Wickland, K. P., French, N., Waldrop, M., Bourgeau-Chavez, L., and Striegl, R. G.: Vulnerability of high-latitude soil organic carbon in North America to disturbance, J. Geophys. Res., 116, G00K06, https://doi.org/10.1029/2010JG001507, 2011.

Guimond, J. A., Mohammed, A. A., Walvoord, M. A., Bense, V. F., and Kurylyk, B. L.: Saltwater Intrusion Intensifies Coastal Permafrost Thaw, Geophysical Research Letters, 48, e2021GL094776, https://doi.org/10.1029/2021GL094776, 2021.

Guimond, J. A., Mohammed, A. A., Walvoord, M. A., Bense, V. F., and Kurylyk, B. L.: Sea-level rise and warming mediate coastal groundwater discharge in the Arctic, Environ. Res. Lett., 17, 045027, https://doi.org/10.1088/1748-9326/ac6085, 2022.

Harris, C. M., McClelland, J. W., Connelly, T. L., Crump, B. C., and Dunton, K. H.: Salinity and Temperature Regimes in Eastern Alaskan Beaufort Sea Lagoons in Relation to Source Water Contributions, Estuaries and Coasts, 40, 50–62, https://doi.org/10.1007/s12237-016-0123-z, 2017.

Haugk, C., Jongejans, L. L., Mangelsdorf, K., Fuchs, M., Ogneva, O., Palmtag, J., Mollenhauer, G., Mann, P. J., Overduin, P. P., Grosse, G., Sanders, T., Tuerena, R. E., Schirrmeister, L., Wetterich, S., Kizyakov, A., Karger, C., and Strauss, J.: Organic matter characteristics of a rapidly eroding permafrost cliff in NE Siberia (Lena Delta, Laptev Sea region), Biogeosciences, 19, 2079–2094, https://doi.org/10.5194/bg-19-2079-2022, 2022.

Hinkel, K. M., Eisner, W. R., Bockheim, J. G., Nelson, F. E., Peterson, K. M., and Dai, X.: Spatial Extent, Age, and Carbon Stocks in Drained Thaw Lake Basins on the Barrow Peninsula, Alaska, Arctic, Antarctic, and Alpine Research, 35, 291–300, https://doi.org/10.1657/1523-0430(2003)035%5B0291:SEAACS%5D2.0.CO;2, 2003.

Hinkel, K. M., Frohn, R. C., Nelson, F. E., Eisner, W. R., and Beck, R. A.: Morphometric and spatial analysis of thaw lakes and drained thaw lake basins in the western Arctic Coastal Plain, Alaska, Permafrost and Periglacial Processes, 16, 327–341, https://doi.org/10.1002/ppp.532, 2005.

Irrgang, A. M., Bendixen, M., Farquharson, L. M., Baranskaya, A. V., Erikson, L. H., Gibbs, A. E., Ogorodov, S. A., Overduin, P. P., Lantuit, H., Grigoriev, M. N., and Jones, B. M.: Drivers, dynamics and impacts of changing Arctic coasts, Nat Rev Earth Environ, 3, 39–54, https://doi.org/10.1038/s43017-021-00232-1, 2022.

Jenrich, M., Angelopoulos, M., Grosse, G., Overduin, P. P., Schirrmeister, L., Nitze, I., Biskaborn, B. K., Liebner, S., Grigoriev, M., Murray, A., Jongejans, L. L., and Strauss, J.: Thermokarst lagoons: A core-based assessment of depositional characteristics and an estimate of carbon pools on the Bykovsky Peninsula, Frontiers in Earth Science, 9, 2021.

Jenrich, M., Angelopoulos, M., Liebner, S., Treat, C., Knoblauch, C., Yang, S., Grosse, G., Giebeler, F., Jongejans, L. L., Grigoriev, M., and Strauss, J.: Greenhouse Gas Production and Microbial Response During the Transition From Terrestrial Permafrost to a Marine Environment, Permafrost and Periglacial Processes, 36, 63–82, https://doi.org/10.1002/ppp.2251, 2024.

Jenrich, M., Wolter, J., Liebner, S., Knoblauch, C., Grosse, G., Giebeler, F., Whalen, D., and Strauss, J.: Rising Arctic seas and thawing permafrost: uncovering the carbon cycle impact in a thermokarst lagoon system in the outer Mackenzie Delta, Canada, Biogeosciences, 22, 2069–2086, https://doi.org/10.5194/bg-22-2069-2025, 2025a.

Jenrich, M., Prodinger, M., Nitze, I., Grosse, G., and Strauss, J.: Thermokarst Lagoons: Distribution, Classification and Dynamics in Permafrost-to-Marine Transitions, Permafrost and Periglacial Processes, n/a, https://doi.org/10.1002/ppp.70001, 2025b.

Jones, B. M., Arp, C. D., Grosse, G., Nitze, I., Lara, M. J., Whitman, M. S., Farquharson, L. M., Kanevskiy, M., Parsekian, A. D., Breen, A. L., Ohara, N., Rangel, R. C., and Hinkel, K. M.: Identifying historical and future potential lake drainage events on the western Arctic coastal plain of Alaska, Permafrost and Periglac Process, 31, 110–127, https://doi.org/10.1002/ppp.2038, 2020.

Jones, B. M., Grosse, G., Farquharson, L. M., Roy-Léveillée, P., Veremeeva, A., Kanevskiy, M. Z., Gaglioti, B. V., Breen, A. L., Parsekian, A. D., Ulrich, M., and Hinkel, K. M.: Lake and drained lake basin systems in lowland permafrost regions, Nat Rev Earth Environ, 3, 85–98, https://doi.org/10.1038/s43017-021-00238-9, 2022.

Jones, B. M., Kanevskiy, M. Z., Parsekian, A. D., Bergstedt, H., Ward Jones, M. K., Rangel, R. C., Hinkel, K. M., and Shur, Y.: Rapid Saline Permafrost Thaw Below a Shallow Thermokarst Lake in Arctic Alaska, Geophysical Research Letters, 50, e2023GL105552, https://doi.org/10.1029/2023GL105552, 2023.

Jones, M. C. and Yu, Z.: Rapid deglacial and early Holocene expansion of peatlands in Alaska, Proceedings of the National Academy of Sciences, 107, 7347–7352, https://doi.org/10.1073/pnas.0911387107, 2010.

Jones, M. C., Grosse, G., Jones, B. M., and Walter Anthony, K. M.: Peat accumulation in drained thermokarst lake basins in continuous, ice-rich permafrost, northern Seward Peninsula, Alaska, J. Geophys. Res., 117, https://doi.org/10.1029/2011JG001766, 2012.

Jong, D., Bröder, L., Tesi, T., Tanski, G., Oudenhuijsen, M., Fritz, M., Lantuit, H., Haghipour, N., Eglinton, T., and Vonk, J.: Selective Sorting and Degradation of Permafrost Organic Matter in the Nearshore Zone of Herschel Island (Yukon, Canada), Journal of Geophysical Research: Biogeosciences, 129, e2023JG007479, https://doi.org/10.1029/2023JG007479, 2024.

Jongejans, L. L., Mangelsdorf, K., Schirrmeister, L., Grigoriev, M. N., Maksimov, G. M., Biskaborn, B. K., Grosse, G., and Strauss, J.: n-Alkane Characteristics of Thawed Permafrost Deposits Below a Thermokarst Lake on Bykovsky Peninsula, Northeastern Siberia, Front. Environ. Sci., 8, 118, https://doi.org/10.3389/fenvs.2020.00118, 2020.

Jongejans, L. L., Liebner, S., Knoblauch, C., Mangelsdorf, K., Ulrich, M., Grosse, G., Tanski, G., Fedorov, A. N., Konstantinov, P. Ya., Windirsch, T., Wiedmann, J., and Strauss, J.: Greenhouse gas production and lipid biomarker distribution in Yedoma and Alas thermokarst lake sediments in Eastern Siberia, Global Change Biology, 27, 2822–2839, https://doi.org/10.1111/gcb.15566, 2021.

Kaufman, D. S., Ager, T. A., Anderson, N. J., Anderson, P. M., Andrews, J. T., Bartlein, P. J., Brubaker, L. B., Coats, L. L., Cwynar, L. C., Duvall, M. L., Dyke, A. S., Edwards, M. E., Eisner, W. R., Gajewski, K., Geirsdóttir, A., Hu, F. S., Jennings, A. E., Kaplan, M. R., Kerwin, M. W., Lozhkin, A. V., MacDonald, G. M., Miller, G. H., Mock, C. J., Oswald, W. W., Otto-Bliesner, B. L., Porinchu, D. F., Rühland, K., Smol, J. P., Steig, E. J., and Wolfe, B. B.: Holocene thermal maximum in the western Arctic (0–180°W), Quaternary Science Reviews, 23, 529–560, https://doi.org/10.1016/j.quascirev.2003.09.007, 2004.

Killops, S. D. and Killops, V. J.: Introduction to organic geochemistry, 2nd ed., Blackwell Pub, Malden, MA, 393 pp., 2005.

Lantz, T. C., Zhang, Y., and Kokelj, S. V.: Impacts of ecological succession and climate warming on permafrost aggradation in drained lake basins of the Tuktoyaktuk Coastlands, Northwest Territories, Canada, Permafrost & Periglacial, 33, 176–192, https://doi.org/10.1002/ppp.2143, 2022.

Lara, M. J., McGuire, A. D., Euskirchen, E. S., Tweedie, C. E., Hinkel, K. M., Skurikhin, A. N., Romanovsky, V. E., Grosse, G., Bolton, W. R., and Genet, H.: Polygonal tundra geomorphological change in response to warming alters future CO2 and CH4 flux on the Barrow Peninsula, Global Change Biology, 21, 1634–1651, https://doi.org/10.1111/gcb.12757, 2015.

Lara, M. J., McGuire, A. D., Euskirchen, E. S., Genet, H., Yi, S., Rutter, R., Iversen, C., Sloan, V., and Wullschleger, S. D.: Local-scale Arctic tundra heterogeneity affects regional-scale carbon dynamics, Nat Commun, 11, 4925, https://doi.org/10.1038/s41467-020-18768-z, 2020.

Lara, M. J., Michaelides, R., Anderson, D., Chen, W., Hall, E. C., Ludden, C., Schore, A. I. G., Mishra, U., and Scott, S. N.: A 20 m spatial resolution peatland extent map of Alaska, Sci Data, 12, 226, https://doi.org/10.1038/s41597-025-04502-1, 2025.

Lenz, J., Jones, B. M., Wetterich, S., Tjallingii, R., Fritz, M., Arp, C. D., Rudaya, N., and Grosse, G.: Impacts of shore expansion and catchment characteristics on lacustrine thermokarst records in permafrost lowlands, Alaska Arctic Coastal Plain, Arktos, 2, 25, https://doi.org/10.1007/s41063-016-0025-0, 2016.

Li, M., Li, Z., Dong, S., Chen, L., Su, X., Lu, C., Zhou, A., and Wang, N.: Salinity impacts on n-alkanes in lake sediments of the Badain Jaran Desert, Northwestern China: Implications for paleoclimate reconstruction, Palaeogeography, Palaeoclimatology, Palaeoecology, 656, 112571, https://doi.org/10.1016/j.palaeo.2024.112571, 2024.

Ling, F. and Zhang, T.: Modeling study of talik freeze-up and permafrost response under drained thaw lakes on the Alaskan Arctic Coastal Plain, Journal of Geophysical Research: Atmospheres, 109, https://doi.org/10.1029/2003JD003886, 2004.

Lisiecki, L. E. and Herbert, T. D.: Automated composite depth scale construction and estimates of sediment core extension, Paleoceanography, 22, https://doi.org/10.1029/2006PA001401, 2007.

Liu, Z., Kimball, J. S., Ballantyne, A., Watts, J. D., Natali, S. M., Rogers, B. M., Yi, Y., Klene, A. E., Moghaddam, M., Du, J., and Zona, D.: Widespread deepening of the active layer in northern permafrost regions from 2003 to 2020, Environ. Res. Lett., 19, 014020, https://doi.org/10.1088/1748-9326/ad0f73, 2024.

Lougheed, V. L., Tweedie, C. E., Andresen, C. G., Armendariz, A. M., Escarzaga, S. M., and Tarin, G.: Patterns and Drivers of Carbon Dioxide Concentrations in Aquatic Ecosystems of the Arctic Coastal Tundra, Global Biogeochemical Cycles, 34, e2020GB006552, https://doi.org/10.1029/2020GB006552, 2020.

Maffei, M.: Chemotaxonomic significance of leaf wax alkanes in the gramineae, Biochemical Systematics and Ecology, 24, 53–64, https://doi.org/10.1016/0305-1978(95)00102-6, 1996.

Martens, J., Mueller, C. W., Joshi, P., Rosinger, C., Maisch, M., Kappler, A., Bonkowski, M., Schwamborn, G., Schirrmeister, L., and Rethemeyer, J.: Stabilization of mineral-associated organic carbon in Pleistocene permafrost, Nat Commun, 14, 2120, https://doi.org/10.1038/s41467-023-37766-5, 2023.

Marzi, R., Torkelson, B. E., and Olson, R. K.: A revised carbon preference index, Organic Geochemistry, 20, 1303–1306, https://doi.org/10.1016/0146-6380(93)90016-5, 1993.

McGuire, A. D., Koven, C., Lawrence, D. M., Clein, J. S., Xia, J., Beer, C., Burke, E., Chen, G., Chen, X., Delire, C., Jafarov, E., MacDougall, A. H., Marchenko, S., Nicolsky, D., Peng, S., Rinke, A., Saito, K., Zhang, W., Alkama, R., Bohn, T. J., Ciais, P., Decharme, B., Ekici, A., Gouttevin, I., Hajima, T., Hayes, D. J., Ji, D., Krinner, G., Lettenmaier, D. P., Luo, Y., Miller, P. A., Moore, J. C., Romanovsky, V., Schädel, C., Schaefer, K., Schuur, E. A. G., Smith, B., Sueyoshi, T., and Zhuang, Q.: Variability in the sensitivity among model simulations of permafrost and carbon dynamics in the permafrost region between 1960 and 2009, Global Biogeochemical Cycles, 30, 1015–1037, https://doi.org/10.1002/2016GB005405, 2016.

Meyer, H., Schirrmeister, L., Andreev, A., Wagner, D., Hubberten, H.-W., Yoshikawa, K., Bobrov, A., Wetterich, S., Opel, T., Kandiano, E., and Brown, J.: Lateglacial and Holocene isotopic and environmental history of northern coastal Alaska –

Results from a buried ice-wedge system at Barrow, Quaternary Science Reviews, 29, 3720–3735, https://doi.org/10.1016/j.quascirev.2010.08.005, 2010.

Meyers, P. A.: Preservation of elemental and isotopic source identification of sedimentary organic matter, Chemical Geology, 114, 289–302, https://doi.org/10.1016/0009-2541(94)90059-0, 1994.

Mollenhauer, G., Grotheer, H., Gentz, T., Bonk, E., and Hefter, J.: Standard operation procedures and performance of the MICADAS radiocarbon laboratory at Alfred Wegener Institute (AWI), Germany, Nuclear Instruments and Methods in Physics Research Section B: Beam Interactions with Materials and Atoms, 496, 45–51, https://doi.org/10.1016/j.nimb.2021.03.016, 2021.

Mu, M., Mu, C., Liu, H., Lei, P., Ge, Y., Zhou, Z., Peng, X., and Ma, T.: Thermokarst lake drainage halves the temperature sensitivity of CH4 release on the Qinghai-Tibet Plateau, Nat Commun, 16, 1992, https://doi.org/10.1038/s41467-025-57356-x, 2025.

Nielsen, D. M., Pieper, P., Barkhordarian, A., Overduin, P., Ilyina, T., Brovkin, V., Baehr, J., and Dobrynin, M.: Increase in Arctic coastal erosion and its sensitivity to warming in the twenty-first century, Nat. Clim. Chang., 12, 263–270, https://doi.org/10.1038/s41558-022-01281-0, 2022.

Nitzbon, J., Schneider von Deimling, T., Aliyeva, M., Chadburn, S. E., Grosse, G., Laboor, S., Lee, H., Lohmann, G., Steinert, N. J., Stuenzi, S. M., Werner, M., Westermann, S., and Langer, M.: No respite from permafrost-thaw impacts in the absence of a global tipping point, Nat. Clim. Chang., 14, 573–585, https://doi.org/10.1038/s41558-024-02011-4, 2024.

Nitze, I., Grosse, G., Jones, B. M., Arp, C. D., Ulrich, M., Fedorov, A., and Veremeeva, A.: Landsat-Based Trend Analysis of Lake Dynamics across Northern Permafrost Regions, Remote Sensing, 9, 640, https://doi.org/10.3390/rs9070640, 2017.

Nyland, K. E., Shiklomanov, N. I., Streletskiy, D. A., Nelson, F. E., Klene, A. E., and Kholodov, A. L.: Long-term Circumpolar Active Layer Monitoring (CALM) program observations in Northern Alaskan tundra, Polar Geography, 44, 167–185, https://doi.org/10.1080/1088937X.2021.1988000, 2021.

Obu, J., Westermann, S., Kääb, A., and Bartsch, A.: Ground Temperature Map, 2000-2016, Northern Hemisphere Permafrost, , https://doi.org/10.1594/PANGAEA.888600, 2018.

Obu, J., Westermann, S., Bartsch, A., Berdnikov, N., Christiansen, H. H., Dashtseren, A., Delaloye, R., Elberling, B., Etzelmüller, B., Kholodov, A., Khomutov, A., Kääb, A., Leibman, M. O., Lewkowicz, A. G., Panda, S. K., Romanovsky, V., Way, R. G., Westergaard-Nielsen, A., Wu, T., Yamkhin, J., and Zou, D.: Northern Hemisphere permafrost map based on TTOP modelling for 2000–2016 at 1 km2 scale, Earth-Science Reviews, 193, 299–316, https://doi.org/10.1016/j.earscirev.2019.04.023, 2019.

Osterkamp, T. E.: Occurrence and potential importance of saline permafrost in Alaska, Workshop on Saline Permafrost, 1989.

Osterkamp, T. E. and Harrison, W. D.: Temperature measurements in subsea permafrost off the coast of Alaska, 4th Canadian Permafrost Conf., 1982.

Osterkamp, T. E. and Harrison, W. D.: Subsea permafrost: Probing, thermal regime and data analysis, U.S. Dep. of Commer., NOAA, Environ. Res. Lab., Boulder, Colorado, US, 1985.

Otto, A. and Simpson, M. J.: Degradation and Preservation of Vascular Plant-derived Biomarkers in Grassland and Forest Soils from Western Canada, Biogeochemistry, 74, 377–409, https://doi.org/10.1007/s10533-004-5834-8, 2005.

Overduin, P. P., Westermann, S., Yoshikawa, K., Haberlau, T., Romanovsky, V., and Wetterich, S.: Geoelectric observations of the degradation of nearshore submarine permafrost at Barrow (Alaskan Beaufort Sea), Journal of Geophysical Research: Earth Surface, 117, https://doi.org/10.1029/2011JF002088, 2012.

Parazoo, N. C., Koven, C. D., Lawrence, D. M., Romanovsky, V., and Miller, C. E.: Detecting the permafrost carbon feedback: talik formation and increased cold-season respiration as precursors to sink-to-source transitions, The Cryosphere, 12, 123–144, https://doi.org/10.5194/tc-12-123-2018, 2018.

Ping, C.-L., Michaelson, G. J., Guo, L., Jorgenson, M. T., Kanevskiy, M., Shur, Y., Dou, F., and Liang, J.: Soil carbon and material fluxes across the eroding Alaska Beaufort Sea coastline, Journal of Geophysical Research: Biogeosciences, 116, https://doi.org/10.1029/2010JG001588, 2011.

Poynter, J. and Eglinton, G.: Molecular composition of three sediments from hole 717c: the Bengal fan, edited by: Cochran, J. R., Stow, D. A. V., and et al., Ocean Drilling Program, https://doi.org/10.2973/odp.proc.sr.116.1990, 1990.

Radke, Matthias., Willsch, Helmut., and Welte, D. H.: Preparative hydrocarbon group type determination by automated medium pressure liquid chromatography, Anal. Chem., 52, 406–411, https://doi.org/10.1021/ac50053a009, 1980.

Rantanen, M., Karpechko, A. Y., Lipponen, A., Nordling, K., Hyvärinen, O., Ruosteenoja, K., Vihma, T., and Laaksonen, A.: The Arctic has warmed nearly four times faster than the globe since 1979, Commun Earth Environ, 3, 1–10, https://doi.org/10.1038/s43247-022-00498-3, 2022.

Rawlins, M. A.: Increasing freshwater and dissolved organic carbon flows to Northwest Alaska's Elson lagoon, Environ. Res. Lett., 16, 105014, https://doi.org/10.1088/1748-9326/ac2288, 2021.

Reimer, P. J., Austin, W. E. N., Bard, E., Bayliss, A., Blackwell, P. G., Ramsey, C. B., Butzin, M., Cheng, H., Edwards, R. L., Friedrich, M., Grootes, P. M., Guilderson, T. P., Hajdas, I., Heaton, T. J., Hogg, A. G., Hughen, K. A., Kromer, B., Manning, S. W., Muscheler, R., Palmer, J. G., Pearson, C., Plicht, J. van der, Reimer, R. W., Richards, D. A., Scott, E. M., Southon, J. R., Turney, C. S. M., Wacker, L., Adolphi, F., Büntgen, U., Capano, M., Fahrni, S. M., Fogtmann-Schulz, A., Friedrich, R., Köhler, P., Kudsk, S., Miyake, F., Olsen, J., Reinig, F., Sakamoto, M., Sookdeo, A., and Talamo, S.: The IntCal20 Northern Hemisphere Radiocarbon Age Calibration Curve (0–55 cal kBP), Radiocarbon, 62, 725–757, https://doi.org/10.1017/RDC.2020.41, 2020.

Schäfer, I. K., Lanny, V., Franke, J., Eglinton, T. I., Zech, M., Vysloužilová, B., and Zech, R.: Leaf waxes in litter and topsoils along a European transect, SOIL, 2, 551–564, https://doi.org/10.5194/soil-2-551-2016, 2016.

Schirrmeister, L., Grigoriev, M. N., Strauss, J., Grosse, G., Overduin, P. P., Kholodov, A., Guenther, F., and Hubberten, H.-W.: Sediment characteristics of a thermokarst lagoon in the northeastern Siberian Arctic (Ivashkina Lagoon, Bykovsky Peninsula), Arktos, 4, 1–16, https://doi.org/10.1007/s41063-018-0049-8, 2018.

Schuur, E. A. G., Abbott, B. W., Commane, R., Ernakovich, J., Euskirchen, E., Hugelius, G., Grosse, G., Jones, M., Koven, C., Leshyk, V., Lawrence, D., Loranty, M. M., Mauritz, M., Olefeldt, D., Natali, S., Rodenhizer, H., Salmon, V., Schädel, C., Strauss, J., Treat, C., and Turetsky, M.: Permafrost and Climate Change: Carbon Cycle Feedbacks From the Warming Arctic, Annual Review of Environment and Resources, 47, 343–371, https://doi.org/10.1146/annurev-environ-012220-011847, 2022.

Schwamborn, G., Schirrmeister, L., Mohammadi, A., Meyer, H., Kartoziia, A., Maggioni, F., and Strauss, J.: Fluvial and permafrost history of the lower Lena River, north-eastern Siberia, over late Quaternary time, Sedimentology, 70, 235–258, https://doi.org/10.1111/sed.13037, 2023.

Schwark, L., Zink, K., and Lechterbeck, J.: Reconstruction of postglacial to early Holocene vegetation history in terrestrial Central Europe via cuticular lipid biomarkers and pollen records from lake sediments, Geology, 30, 463–466, https://doi.org/10.1130/0091-7613(2002)030%3C0463:ROPTEH%3E2.0.CO;2, 2002.

Shur, Y., Hinkel, K. M., and Nelson, F. E.: The transient layer: implications for geocryology and climate-change science, Permafrost and Periglacial Processes, 16, 5–17, https://doi.org/10.1002/ppp.518, 2005.

Smith, S. L., O'Neill, H. B., Isaksen, K., Noetzli, J., and Romanovsky, V. E.: The changing thermal state of permafrost, Nat Rev Earth Environ, 3, 10–23, https://doi.org/10.1038/s43017-021-00240-1, 2022.

Strauss, J., Schirrmeister, L., Mangelsdorf, K., Eichhorn, L., Wetterich, S., and Herzschuh, U.: Organic-matter quality of deep permafrost carbon – a study from Arctic Siberia, Biogeosciences, 12, 2227–2245, https://doi.org/10.5194/bg-12-2227-2015, 2015.

Strauss, J., Biasi, C., Sanders, T., Abbott, B. W., von Deimling, T. S., Voigt, C., Winkel, M., Marushchak, M. E., Kou, D., Fuchs, M., Horn, M. A., Jongejans, L. L., Liebner, S., Nitzbon, J., Schirrmeister, L., Walter Anthony, K., Yang, Y., Zubrzycki, S., Laboor, S., Treat, C., and Grosse, G.: A globally relevant stock of soil nitrogen in the Yedoma permafrost domain, Nat Commun, 13, 6074, https://doi.org/10.1038/s41467-022-33794-9, 2022.

Strauss, J., Fuchs, M., Hugelius, G., Miesner, F., Nitze, I., Opfergelt, S., Schuur, E., Treat, C., Turetsky, M., Yang, Y., and Grosse, G.: Organic matter storage and vulnerability in the permafrost domain, in: Encyclopedia of Quaternary Science, Elsevier, 399–410, https://doi.org/10.1016/B978-0-323-99931-1.00164-1, 2025.

Struck, J., Roettig, C. B., Faust, D., and Zech, R.: Leaf waxes from aeolianite–paleosol sequences on Fuerteventura and their potential for paleoenvironmental and climate reconstructions in the arid subtropics, E&G Quaternary Science Journal, 66, 109–114, https://doi.org/10.5194/egqsj-66-109-2018, 2018.

Stuiver, M. and Reimer, P. J.: Extended 14C Data Base and Revised CALIB 3.0 14C Age Calibration Program, Radiocarbon, 35, 215–230, https://doi.org/10.1017/S0033822200013904, 1993.

Thomas, C. L., Jansen, B., van Loon, E. E., and Wiesenberg, G. L. B.: Transformation of n-alkanes from plant to soil: a review, SOIL, 7, 785–809, https://doi.org/10.5194/soil-7-785-2021, 2021.

Tipple, B. J. and Pagani, M.: A 35 Myr North American leaf-wax compound-specific carbon and hydrogen isotope record: Implications for C4 grasslands and hydrologic cycle dynamics, Earth and Planetary Science Letters, 299, 250–262, https://doi.org/10.1016/j.epsl.2010.09.006, 2010.

Ulyantsev, A. S., Romankevich, E. A., Bratskaya, S. Yu., Prokuda, N. A., Sukhoverkhov, S. V., Semiletov, I. P., and Sergienko, V. I.: Characteristic of quaternary sedimentation on a shelf of the Laptev Sea according to the molecular composition of n-alkanes, Dokl. Earth Sc., 473, 449–453, https://doi.org/10.1134/S1028334X17040158, 2017.

Vonk, J. E., Fritz, M., Speetjens, N. J., Babin, M., Bartsch, A., Basso, L. S., Bröder, L., Göckede, M., Gustafsson, Ö., Hugelius, G., Irrgang, A. M., Juhls, B., Kuhn, M. A., Lantuit, H., Manizza, M., Martens, J., O'Regan, M., Suslova, A., Tank, S. E., Terhaar, J., and Zolkos, S.: The land–ocean Arctic carbon cycle, Nat Rev Earth Environ, 6, 86–105, https://doi.org/10.1038/s43017-024-00627-w, 2025.

Walter Anthony, K. M., Zimov, S. A., Grosse, G., Jones, M. C., Anthony, P. M., Iii, F. S. C., Finlay, J. C., Mack, M. C., Davydov, S., Frenzel, P., and Frolking, S.: A shift of thermokarst lakes from carbon sources to sinks during the Holocene epoch, Nature, 511, 452–456, https://doi.org/10.1038/nature13560, 2014.

Webb, E. E., Liljedahl, A. K., Cordeiro, J. A., Loranty, M. M., Witharana, C., and Lichstein, J. W.: Permafrost thaw drives surface water decline across lake-rich regions of the Arctic, Nat. Clim. Chang., 12, 841–846, https://doi.org/10.1038/s41558-022-01455-w, 2022.

Webb, H., Fuchs, M., Abbott, B. W., Douglas, T. A., Elder, C. D., Ernakovich, J. G., Euskirchen, E. S., Göckede, M., Grosse, G., Hugelius, G., Jones, M. C., Koven, C., Kropp, H., Lathrop, E., Li, W., Loranty, M. M., Natali, S. M., Olefeldt, D., Schädel, C., Schuur, E. A. G., Sonnentag, O., Strauss, J., Virkkala, A.-M., and Turetsky, M. R.: A Review of Abrupt Permafrost Thaw: Definitions, Usage, and a Proposed Conceptual Framework, Curr Clim Change Rep, 11, 7, https://doi.org/10.1007/s40641-025-00204-3, 2025.

Weber, J. and Schwark, L.: Epicuticular wax lipid composition of endemic European Betula species in a simulated ontogenetic/diagenetic continuum and its application to chemotaxonomy and paleobotany, Science of The Total Environment, 730, 138324, https://doi.org/10.1016/j.scitotenv.2020.138324, 2020.

Wolter, J., Lantuit, H., Herzschuh, U., Stettner, S., and Fritz, M.: Tundra vegetation stability versus lake-basin variability on the Yukon Coastal Plain (NW Canada) during the past three centuries, The Holocene, 27, 1846–1858, https://doi.org/10.1177/0959683617708441, 2017.

Wolter, J., Jones, B. M., Fuchs, M., Breen, A., Bussmann, I., Koch, B., Lenz, J., Myers-Smith, I. H., Sachs, T., Strauss, J., Nitze, I., and Grosse, G.: Post-drainage vegetation, microtopography and organic matter in Arctic drained lake basins, Environ. Res. Lett., 19, 045001, https://doi.org/10.1088/1748-9326/ad2eeb, 2024.

Wu, J., Mollenhauer, G., Stein, R., Köhler, P., Hefter, J., Fahl, K., Grotheer, H., Wei, B., and Nam, S.-I.: Deglacial release of petrogenic and permafrost carbon from the Canadian Arctic impacting the carbon cycle, Nat Commun, 13, 7172, https://doi.org/10.1038/s41467-022-34725-4, 2022.

Yang, S., Anthony, S. E., Jenrich, M., in 't Zandt, M. H., Strauss, J., Overduin, P. P., Grosse, G., Angelopoulos, M., Biskaborn, B. K., Grigoriev, M. N., Wagner, D., Knoblauch, C., Jaeschke, A., Rethemeyer, J., Kallmeyer, J., and Liebner, S.: Microbial methane cycling in sediments of Arctic thermokarst lagoons, Global Change Biology, 29, 2714–2731, https://doi.org/10.1111/gcb.16649, 2023.

Zech, M., Andreev, A., Zech, R., Müller, S., Hambach, U., Frechen, M., and Zech, W.: Quaternary vegetation changes derived from a loess-like permafrost palaeosol sequence in northeast Siberia using alkane biomarker and pollen analyses, Boreas, 39, 540–550, https://doi.org/10.1111/j.1502-3885.2009.00132.x, 2010.

Zech, M., Lerch, M., Bliedtner, M., Bromm, T., Seemann, F., Szidat, S., Salazar, G., Zech, R., Glaser, B., Haas, J. N., Schäfer, D., and Geitner, C.: Revisiting the subalpine Mesolithic site Ullafelsen in the Fotsch Valley, Stubai Alps, Austria – new insights into pedogenesis and landscape evolution from leaf-wax-derived n-alkanes, black carbon and radiocarbon dating, E&G Quaternary Sci. J., 70, 171–186, https://doi.org/10.5194/egqsj-70-171-2021, 2021.

Zimmermann, M., Erikson, L. H., Gibbs, A. E., Prescott, M. M., Escarzaga, S. M., Tweedie, C. E., Kasper, J. L., and Duvoy, P. X.: Nearshore bathymetric changes along the Alaska Beaufort Sea coast and possible physical drivers, Continental Shelf Research, 242, 104745, https://doi.org/10.1016/j.csr.2022.104745, 2022.